Cell Genomics

Article

Multi-omic underpinnings of heterogeneous aging across multiple organ systems

Graphical abstract

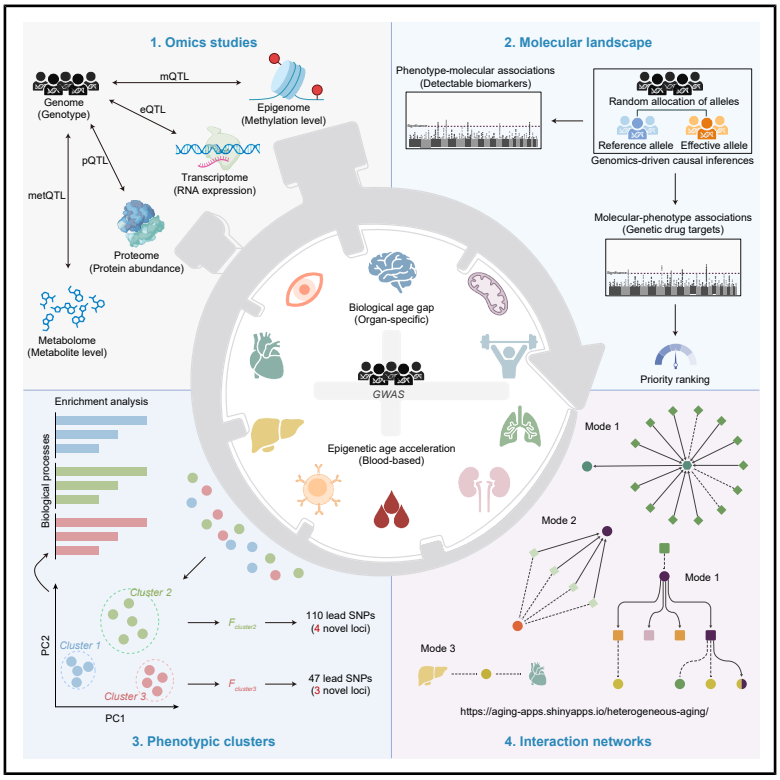

Highlights

- Heterogeneous aging phenotypic clusters exhibit distinct biological signatures
- Genomics-driven approaches identify prioritized drug targets for heterogeneous aging
- Downstream proteomic and metabolomic effects reveal biomarkers of heterogeneous aging
- Integrative findings elucidate cross-layer interaction networks of heterogeneous aging

Authors

Jie Xiong, Xiaoting Zhu, Yutong Guo, ..., Mengran Liu, Zhaoyue Li, Yingfeng Tu

Correspondence

zhaoyuelidr@163.com (Z.L.), tyfdoctor@hrbmu.edu.cn (Y.T.)

In brief

Xiong et al. integrated genetic analysis of multi-omics data with GWASs to construct a comprehensive molecular landscape of nine organ-specific aging clocks and four blood-based epigenetic clocks. This landscape elucidates heterogeneous aging phenotypic clusters and cross-layer interaction networks underlying heterogeneous aging, contributing to a paradigm shift in age-related disease management strategies.

Xiong et al., 2025, Cell Genomics 5, 101032
December 10, 2025
https://doi.org/10.1016/j.xgen.2025.101032

CellPress

Cell Genomics

CellPress
OPEN ACCESS

Article

Multi-omic underpinnings of heterogeneous aging across multiple organ systems

Jie Xiong,[1] Xiaoting Zhu,[2] Yutong Guo,[1] Hao Tang,[3] Chengji Dong,[4] Bo Wang,[1] Mengran Liu,[1] Zhaoyue Li,[5,*] and Yingfeng Tu[1,6,7,*]

[1]Department of Cardiology, The First Affiliated Hospital, Harbin Medical University, Harbin 150000, China
[2]Department of Anesthesiology, The First Affiliated Hospital of Jiamusi University, Jiamusi 154000, China
[3]Department of Cardiology, Huzhou Central Hospital, Fifth School of Clinical Medicine of Zhejiang Chinese Medical University, Huzhou 313000, China
[4]Department of Gastroenterology, Hepatology, Infectious Diseases and Endocrinology, Hannover Medical School, 30625 Hannover, Germany
[5]Department of Cardiology, Affiliated Hospital of Yangzhou University, Yangzhou University, Yangzhou Key Lab of Innovation Frontiers in Cardiovascular Disease, Yangzhou 225000, China
[6]Department of Cardiology, The Shanxi Provincial People's Hospital Affiliated to Shanxi Medical University, Taiyuan 030000, China
[7]Lead contact
*Correspondence: zhaoyuelidr@163.com (Z.L.), tyfdoctor@hrbmu.edu.cn (Y.T.)
https://doi.org/10.1016/j.xgen.2025.101032

SUMMARY

Aging is the main determinant of chronic diseases and mortality, yet organ-specific aging trajectories vary, and the molecular basis underlying this heterogeneity remains unclear. To elucidate this, we integrated genomic, epigenomic, transcriptomic, proteomic, and metabolomic data, employing post-genome-wide association study methodologies to systematically investigate the molecular mechanisms of nine organ-specific aging clocks and four blood-based epigenetic clocks. We uncovered genetic correlations and specific phenotypic clusters among these aging-related traits, identified prioritized genetic drug targets for heterogeneous aging, and elucidated downstream proteomic and metabolomic effects mediated by heterogeneous aging. We constructed a cross-layer molecular interaction network of heterogeneous aging across multiple organ systems and characterized detectable biomarkers of this heterogeneity. Integrating these findings, we developed an R/Shiny-based framework that provides a comprehensive multi-omic molecular landscape of heterogeneous aging, thereby advancing the understanding of aging heterogeneity and informing precision medicine strategies to delay organ-specific aging and prevent or treat its associated chronic diseases.

INTRODUCTION

Aging, a complex biological process characterized by the gradual deterioration of various systems and organs in the body, is a major determinant for most common chronic diseases and causes of death.[1] Historically, medical interventions have primarily focused on preventing, diagnosing, and treating specific age-related diseases. However, advances in aging biology suggest that these diseases epitomize accelerated organ- and system-specific aging.[2] Therefore, targeting aging itself as a shared root cause of disease through universal whole-organism and personalized organ-specific anti-aging therapeutic strategies may yield health and economic benefits far surpassing those of disease-specific treatments.[3,4] Nevertheless, translating this concept into practice still faces significant challenges due to limited understanding of the molecular mechanisms of aging and its potential therapeutic targets.

DNA methylation (DNAm)-based epigenetic clocks are among the earliest and most widely studied aging biomarkers.[5] As biomarkers of single-tissue or pan-tissue aging, they can be utilized to predict chronological age and/or age-related endpoints.[6–9] The development of organ-specific aging clocks has revealed significantly heterogeneous aging trajectories across human organ systems, and biological aging in one organ may selectively influence the aging processes of other organs through potential interaction networks.[2,10] However, the molecular mechanisms underlying differences in organ and tissue aging rates within individuals remain unclear. Given the immense clinical potential of delaying biological aging, elucidating the interaction networks mediating epigenetic aging and organ-specific aging, along with identifying molecular targets capable of modulating these heterogeneous aging processes, will greatly facilitate the paradigm shift in age-related disease management strategies from "divide and treat" to "unite and prevent."

Advances in genome-wide association studies (GWASs) and post-GWAS methodologies have provided powerful tools to decipher molecular mechanisms and discover drug targets for complex traits and diseases.[11] Over the past decade, large-scale molecular quantitative trait locus (QTL) datasets have systematically characterized the genetic regulation of DNAm, gene expression,

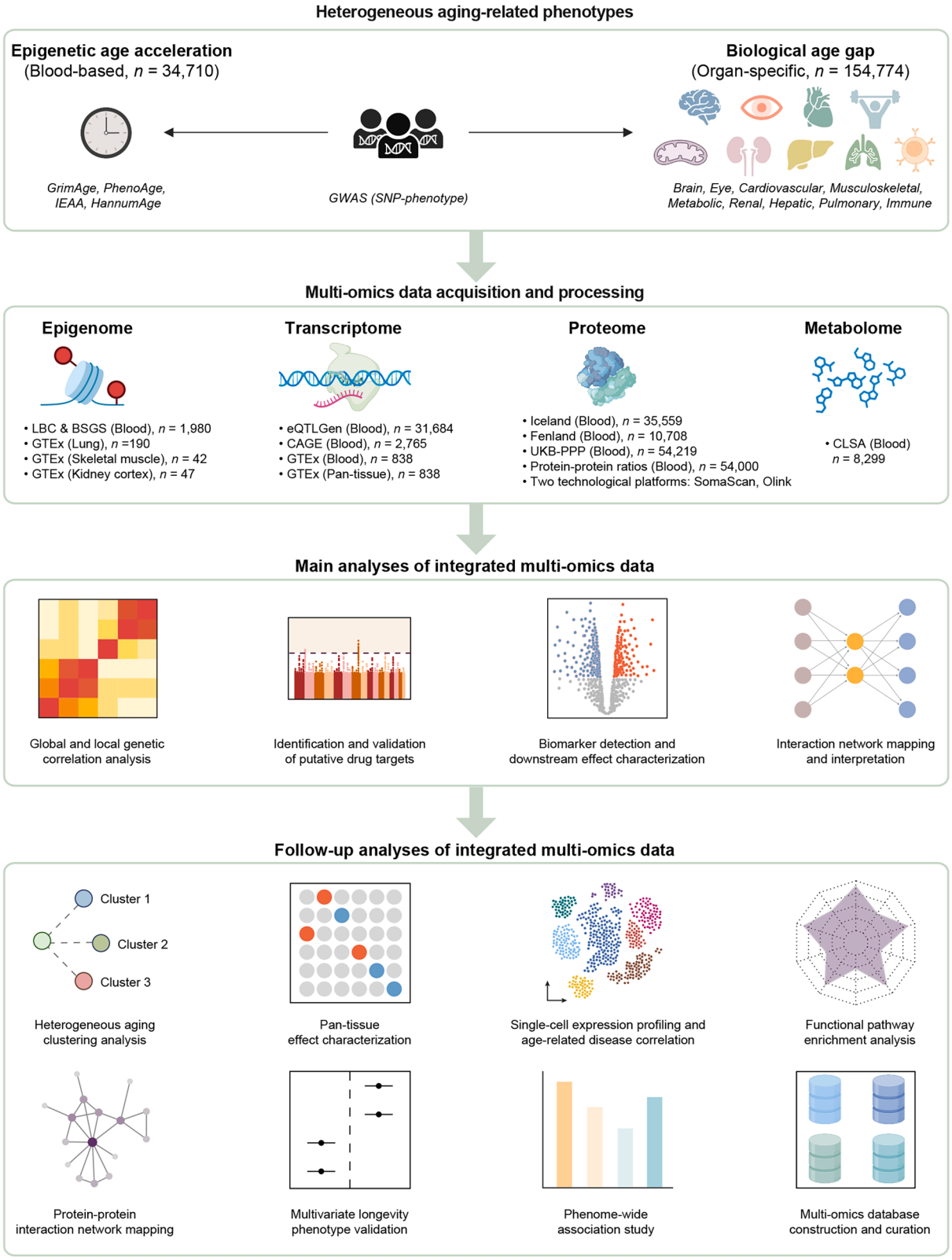

(legend on next page)

protein concentrations, and metabolite levels.[12–18] The availability of these QTL resources presents a unique opportunity to map causal relationships in cross-layer molecular regulatory interaction networks.[19] Furthermore, integrating genetics-based interaction networks with GWAS data helps bridge the molecular mechanistic gap between genetic variations and complex traits.

In this study, we integrated genomic, epigenomic, transcriptomic, proteomic, and metabolomic data and employed post-GWAS methodologies to systematically investigate the cross-layer molecular basis of biological age gap (the difference between machine learning-predicted biological age and chronological age) quantified by nine organ-specific aging clocks and epigenetic age acceleration (the difference between epigenetic age and chronological age) assessed by four blood-based epigenetic clocks (Figure 1). Our objectives are to (1) elucidate genetic correlations between organ-specific aging and blood-based epigenetic aging, uncovering phenotypic clusters associated with heterogeneous aging across multiple organ systems; (2) prioritize candidate genetic drug targets associated with these heterogeneous aging processes and evaluate opportunities for drug repurposing; (3) reveal downstream proteomic and metabolomic effects driven by organ-specific aging and blood-based epigenetic aging, identifying their detectable biomarkers; and (4) integrate findings to map interaction networks of heterogeneous aging across multiple organ systems and their underlying cross-layer molecular regulatory mechanisms. Our findings are publicly accessible through an R/Shiny application (https://aging-apps.shinyapps.io/heterogeneous-aging/) that provides a comprehensive molecular landscape for organ-specific aging and blood-based epigenetic aging, unveiling the multi-omics underpinnings of heterogeneous aging. These insights are expected to advance both basic and translational research, promoting the development of innovative therapeutic strategies aimed at extending healthspan.

RESULTS

Genetic correlations within and between blood-based epigenetic age acceleration and organ-specific biological age gap

All 13 aging-related traits exhibited significant SNP-based heritability, laying the foundation for elucidating genetic correlations underlying heterogeneous aging (Tables S1 and S2). Using linkage disequilibrium (LD) score regression, we quantified global genetic correlations among these phenotypes and identified 32 distinct significant phenotype pairs, which revealed an intricate correlation network between blood-based epigenetic age acceleration and organ-specific biological age gap, suggesting multi-strata interactions in aging (Figure S1A; Table S2). Further fine-grained analysis identified 2,403 significant bivariate correlations across 920 semi-independent blocks (Figure S1B; Table S2). Even for phenotype pairs without significant global genetic correlation, at least one locus showed a significant local genetic correlation, indicating that global analyses may overlook the fine-scale heterogeneity. For traits with significant global genetic correlations, most local genetic correlations aligned directionally with genome-wide patterns. Notably, PhenoAge exhibited the largest number of significant local genetic correlations with other phenotypes, suggesting it may capture the broadest aspects of heterogeneous aging. In conclusion, these findings elucidate both genetic homogeneity and heterogeneity in blood-based epigenetic age acceleration and organ-specific biological age gap, highlighting the need to identify phenotype-specific intervention targets, particularly for organ-specific biological age gap, which is distinct from the blood-based epigenetic acceleration.

Proteomic identification of druggable plasma targets for heterogeneous aging-related traits

Proteins, as gene effectors, are prime candidates for pharmacological interventions.[20] Their circulating abundances are often significantly influenced by genetic variations.[16–18] Therefore, we employed SMR and HEIDI methodologies to identify druggable plasma proteins potentially influencing heterogeneous aging-related traits, investigating whether these proteins are associated with phenotypes through shared causal variants.[21] We utilized genetic data for protein QTLs (pQTLs) from three independent cohorts (Iceland, n = 35,559; Fenland, n = 10,708; and UKB-PPP, n = 54,219) based on diverse technological platforms (SomaScan and Olink).[16–18] Association analyses between these data and blood-based epigenetic age acceleration and organ-specific biological age gap identified distinct plasma proteins significantly associated with these aging phenotypes: 6, 27, 2, 29, 16, 36, 18, 29, and 25 proteins for brain, cardiovascular, eye, hepatic, immune, metabolic, musculoskeletal, pulmonary, and renal biological age gaps, respectively, and 2 proteins each for GrimAge and PhenoAge (Figures 2A and S2–S14; Table S3). Several proteins were consistently identified across multiple datasets despite platform diversity, strongly corroborating the robustness and reproducibility of our findings (Figure 2A).

Although the SMR and HEIDI methods identified numerous significant associations, approximately half lacked strong colocalization evidence (PP-H4 > 0.8) (Figures S15A–S15C; Table S3). To mitigate potential false-positive results arising from LD between neighboring signals, we posit that protein-trait associations lacking strong colocalization evidence should not be construed as indicative of direct causality. Applying this stringent criterion, we ultimately identified 2, 9, 2, 14, 7, 14, 3, 8, 11, 1, and 2 plasma proteins associated with each of the aforementioned phenotypes, respectively (Figures 2B and S15D). These identified proteins play pivotal roles in mediating susceptibility to blood-based epigenetic

Figure 1. Overall study design and methodological framework

A schematic representation elucidating the data sources, analytical pipeline, and methodological approach used in this study. Epigenetic age acceleration (the difference between epigenetic age and chronological age) was assessed by four blood-based epigenetic clocks. Biological age gap (the difference between machine learning-predicted biological age and chronological age) was quantified by nine organ-specific aging clocks.

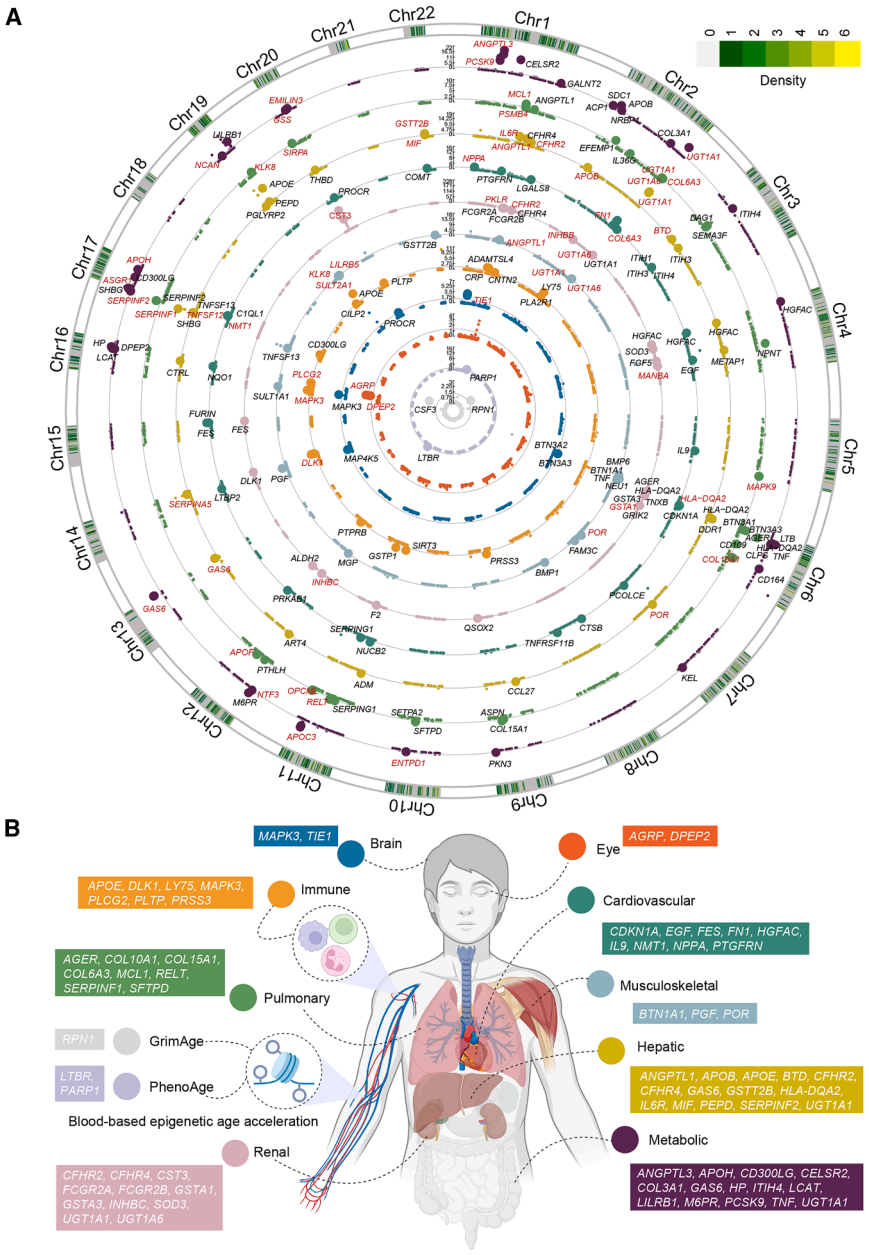

Figure 2. High-priority druggable plasma proteins associated with heterogeneous aging-related phenotypes

(A) Circular Manhattan plot showing putative druggable plasma proteins associated with nine organ-specific biological age gaps and two blood-based epigenetic age accelerations (false discovery rate [FDR]_SMR < 0.05 and *p*_HEIDI > 0.05). Proteins highlighted in red were replicated in independent cohorts.

(B) Putative druggable plasma proteins from (A) supported by colocalization evidence (PP-H4 > 0.8). All proteins are denoted by their corresponding coding genes.

age acceleration and organ-specific biological age gap, potentially serving as high-priority druggable targets for attenuating heterogeneous aging processes and treating age-related diseases.

Transcriptomic and epigenomic landscapes of heterogeneous aging-related traits

To further elucidate the relationship between genetic variants and heterogeneous aging-associated phenotypes, we extended the SMR and HEIDI framework to transcriptome and epigenome data. Transcriptome analysis used expression QTL (eQTL) summary statistics from three complementary cohorts: eQTLGen Consortium data (n = 31,684), Consortium for the Architecture of Gene Expression (CAGE) data (n = 2,765), and the Genotype-Tissue Expression (GTEx) project (n = 838).[13–15] SMR and HEIDI identified potentially druggable genes ranging from 3 to 45 that were significantly associated with biological age gap across nine organ systems and 1 to 5 genes significantly associated with epigenetic age acceleration, including GrimAge, HannumAge, intrinsic epigenetic age acceleration (IEAA), and PhenoAge (Figures S16–S28; Table S4). Colocalization analysis further refined these findings, revealing high-priority druggable genes with strong evidence of linkage to all assessed phenotypes (Figure S29; Table S4). Epigenome analysis used methylation QTL (mQTL) summary statistics from a meta-analysis of two blood-based cohorts: Brisbane Systems Genetics Study (BSGS; n = 614) and Lothian Birth Cohorts (LBC; n = 1,366).[12] SMR and HEIDI identified between 1 and 339 distinct DNAm sites significantly associated with organ-specific biological age gap and blood-based epigenetic age acceleration (Figures S30–S41; Table S5). Subsequent colocalization analysis confirmed subsets of these associations, with immune biological age gap showing the most (149 sites corresponding to 35 nearest genes) and PhenoAge the fewest (1 site corresponding to 1 nearest gene) (Figure S43A; Table S5). To assess tissue specificity, we applied the SMR and HEIDI framework to tissue-specific mQTL data from GTEx for three tissues directly corresponding to the aging phenotypes examined in our study: lung (n = 190), skeletal muscle (n = 42), and kidney cortex (n = 47).[22] For pulmonary biological age gap, 102 significant tissue-associated DNAm sites were identified, whereas musculoskeletal and renal biological age gaps yielded only 4 and 1 significant sites, respectively (Figures S42 and S45; Table S5).

We utilized pulmonary biological age gap as a representative example to illustrate our findings. At the transcriptomic level,

SMR and HEIDI identified 45 potentially druggable genes, of which 8 (*SCP2*, *DSTYK*, *GP9*, *CD109*, *KCNH3*, *GDF11*, *DNASE1*, and *CD79B*) showed robust colocalization evidence (Figure 3A; Table S4). At the epigenomic level, analysis of mQTL data from the LBC and BSGS cohorts identified 339 significant DNAm sites, of which 72 passed colocalization testing, mapping to 27 nearest genes, encompassing *SCP2*, *DSTYK*, *EFEMP1*, *HIST1H4K*, *HLA-G*, *HLA-A*, *EHMT2*, *FRK*, *ESR1*, *BLK*, *OBP2B*, *CAMK2G*, *PLAU*, *PPIF*, *AMPD3*, *NTM*, *ERBB3*, *BMP4*, *SSTR5*, *MMP15*, *SERPINF1*, *CRHR1*, *MAPT*, *NOTUM*, *ADAMTS10*, *APOE*, and *RELT* (Figure 3B; Table S5). Tissue-specific analysis using the GTEx resource for pulmonary biological age gap revealed 102 significant tissue-associated DNAm sites, with 46 showing strong colocalization signals and mapping to 21 nearest genes, including *RPS6KA1*, *SCP2*, *KLHL29*, *TGFBR2*, *KALRN*, *TFRC*, *FGFR3*, *CD109*, *FRK*, *COL10A1*, *BRD3*, *COL13A1*, *PPIF*, *AMPD3*, *LOXL1*, *DNASE1*, *TRAP1*, *SERPINF1*, *MAPT*, *WNT3*, and *APOH* (Figure S43B; Table S5). Comparative analyses revealed shared regulatory mechanisms and unique tissue-specific mQTL signals, with 20 DNAm sites representing cross-tissue conserved signatures, 26 representing blood-specific signatures, and 6 representing lung-specific signatures (Figure S44). Most importantly, our multi-omics approach provided converging evidence for *CD109*, *DNASE1*, *COL10A1*, *RELT*, *DSTYK*, *SERPINF1*, and *SCP2* as potential key regulators of pulmonary aging (Figure 3C). Among these, 3 DNAm sites (cg06940127, cg24214470, and cg22513955) associated with *SERPINF1* and 1 site (cg01802117) associated with *SCP2* were identified as cross-tissue shared, whereas cg00857998 associated with *DSTYK* was blood specific (Figure 3D).

Multi-level analysis reveals three phenotypic clusters of heterogeneous aging

Hierarchical clustering of molecular phenotypes across epigenomic, transcriptomic, and proteomic levels revealed three distinct clusters among 13 heterogeneous aging-associated traits (Figures 4A–4C). The four blood-based epigenetic aging phenotypes consistently grouped into cluster 1 across all molecular levels. The remaining nine organ-specific aging phenotypes segregated into two functional clusters. At the epigenomic level, cluster 2 comprised brain, eye, cardiovascular, metabolic, immune, and pulmonary aging signatures, while cluster 3 included hepatic, renal, and musculoskeletal aging signatures (Figure 4A). This clustering pattern remained highly consistent at transcriptomic and proteomic levels, with pulmonary signatures migrating from cluster 2 to cluster 3 (Figures 4B and 4C).

Further analysis revealed distinct biological characteristics among these clusters (Table S6). Cluster 1 showed predominantly downregulated pathways at the transcriptomic level, while cluster 2 exhibited extensive pathway downregulation at the proteomic level (Figure S46). Each cluster displayed enrichment of pathways specific to their constituent organs: cluster 2 was enriched in cardiovascular system regulation, axon development, immune response activation, and metabolic function reconstruction; cluster 3 was enriched in renal system development, muscular system homeostasis, oxygen level response, and peptidase activity. Notably, pathways involving stimulus response, inflammatory response, and immune cell development and activation were enriched across multiple clusters, suggesting these processes may represent conserved biological hallmarks of heterogeneous aging.

To investigate common etiological factors driving multi-organ heterogeneous aging patterns, we employed genomic structural equation modeling (genomic SEM) to construct shared genetic factors ($F_{cluster1}$, $F_{cluster2}$, and $F_{cluster3}$) for the three clusters and conducted multivariate GWAS (Figures 4D–4F). The three genetic factors showed varying SNP association levels. $F_{cluster1}$ identified 7,101,198 associations with an effective sample size of 9,238. $F_{cluster2}$ and $F_{cluster3}$ identified 5,514,617 and 5,514,505 associations, with effective sample sizes of 386,115 and 328,223, respectively. LD score intercepts, with the exception of $F_{cluster1}$ (intercept = 0.0455, SE = 0.0003), were close to 1 for $F_{cluster2}$ (intercept = 0.9989, SE = 0.0109) and $F_{cluster3}$ (intercept = 0.9891, SE = 0.0098), suggesting no substantial genomic inflation in the latter two multivariate GWASs. For $F_{cluster2}$ and $F_{cluster3}$, we identified 110 and 47 lead SNPs in 61 and 28 genomic loci ($p < 5 \times 10^{-8}$), respectively, of which 4 and 3 were novel discoveries relative to their univariate GWAS (Figures 4E and 4F; Table S7). Q_{SNP} heterogeneity testing showed that 16 SNPs in $F_{cluster2}$ and 28 in $F_{cluster3}$ were heterogeneous ($p < 5 \times 10^{-8}$), whereas none of the novel SNPs displayed heterogeneity, strongly suggesting these loci mediate effects through common genetic factors (Table S7). Fine-mapping analysis further identified 9 causal variants (posterior probability > 0.95), including those located on chromosome 12 ($F_{cluster2}$: rs79880068, an intronic SNP in the *CBX5* locus) and chromosome 2 ($F_{cluster3}$: rs1047891, an exonic SNP in the *CPS1* locus) (Table S8). By extending SMR and HEIDI and colocalization analyses to the common factor level, we prioritized potential drug targets for $F_{cluster2}$ and $F_{cluster3}$, providing novel therapeutic intervention opportunities for multi-organ aging (Figures S47 and S48; Table S9).

Multi-omics integration reveals cross-layer regulatory networks underlying heterogeneous aging

Multi-omics integration analysis facilitates elucidation of cross-layer regulatory pathways across molecular targets, thereby bridging the molecular mechanisms between genetic variation and heterogeneous aging. Using the SMR and HEIDI analytical framework, we systematically revealed causal interaction networks among DNAm sites, gene expression, and protein levels, all of which showed colocalization evidence with heterogeneous aging-related phenotypes (interactive visualization available at https://aging-apps.shinyapps.io/heterogeneous-aging/).

Our analysis revealed synergistic and antagonistic regulatory effects across molecular layers underlying these phenotypes. Taking cardiovascular aging as an example, both *NMT1* transcriptional expression and protein abundance exhibited significant positive correlations with genetic susceptibility (Figure S49A). Within the multi-level regulatory network spanning epigenome, transcriptome, and proteome, we identified 13 key DNAm sites significantly associated with *NMT1* (Figure S49A). Among these, 10 sites (cg00846647, cg16520312, cg16642545, cg16228356, cg24063856, cg21705961, cg05301556, cg05727186, cg23762722, and cg02228913) synergistically upregulated *NMT1* transcription, leading to increased abundance of NMT1

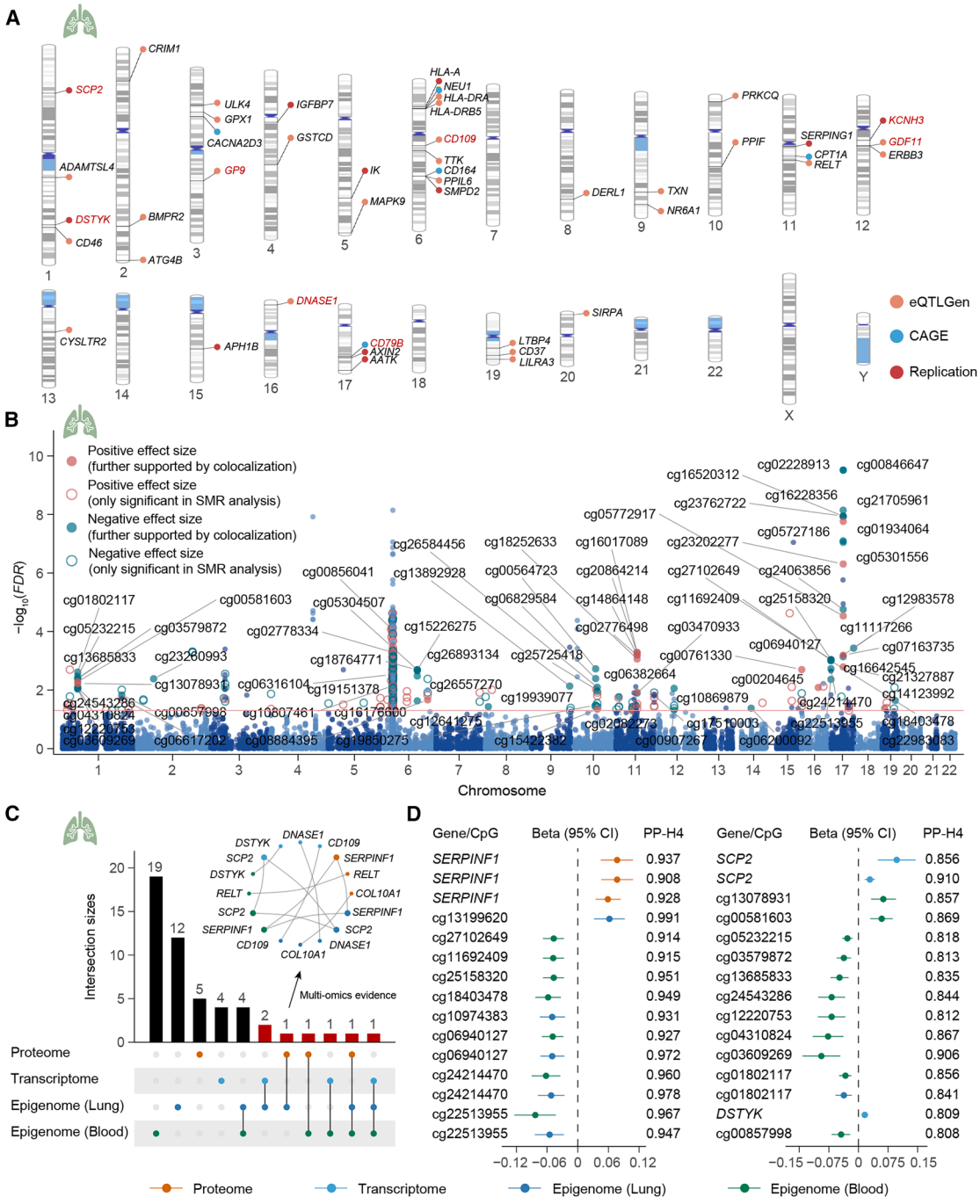

Figure 3. Transcriptomic and epigenomic landscapes associated with pulmonary biological age gap

(A) PhenoGram showing druggable genes significantly associated with pulmonary biological age gap (FDR_SMR < 0.05 and *p*_HEIDI > 0.05). Genes highlighted in red were supported by evidence from colocalization analysis (PP-H4 > 0.8).

(B) Manhattan plot showing DNAm sites significantly associated with pulmonary biological age gap (FDR_SMR < 0.05 and *p*_HEIDI > 0.05).

(C) Upset plot showing the number of shared druggable genes across omics layers (FDR_SMR < 0.05 and *p*_HEIDI > 0.05 and PP-H4 > 0.8), with the inset network diagram showing druggable genes supported by multi-omics evidence.

(D) Forest plot showing proteomics, transcriptomics, and epigenomics evidence for *SERPINF1*, *SCP2*, and *DSTYK* associations with pulmonary biological age gap.

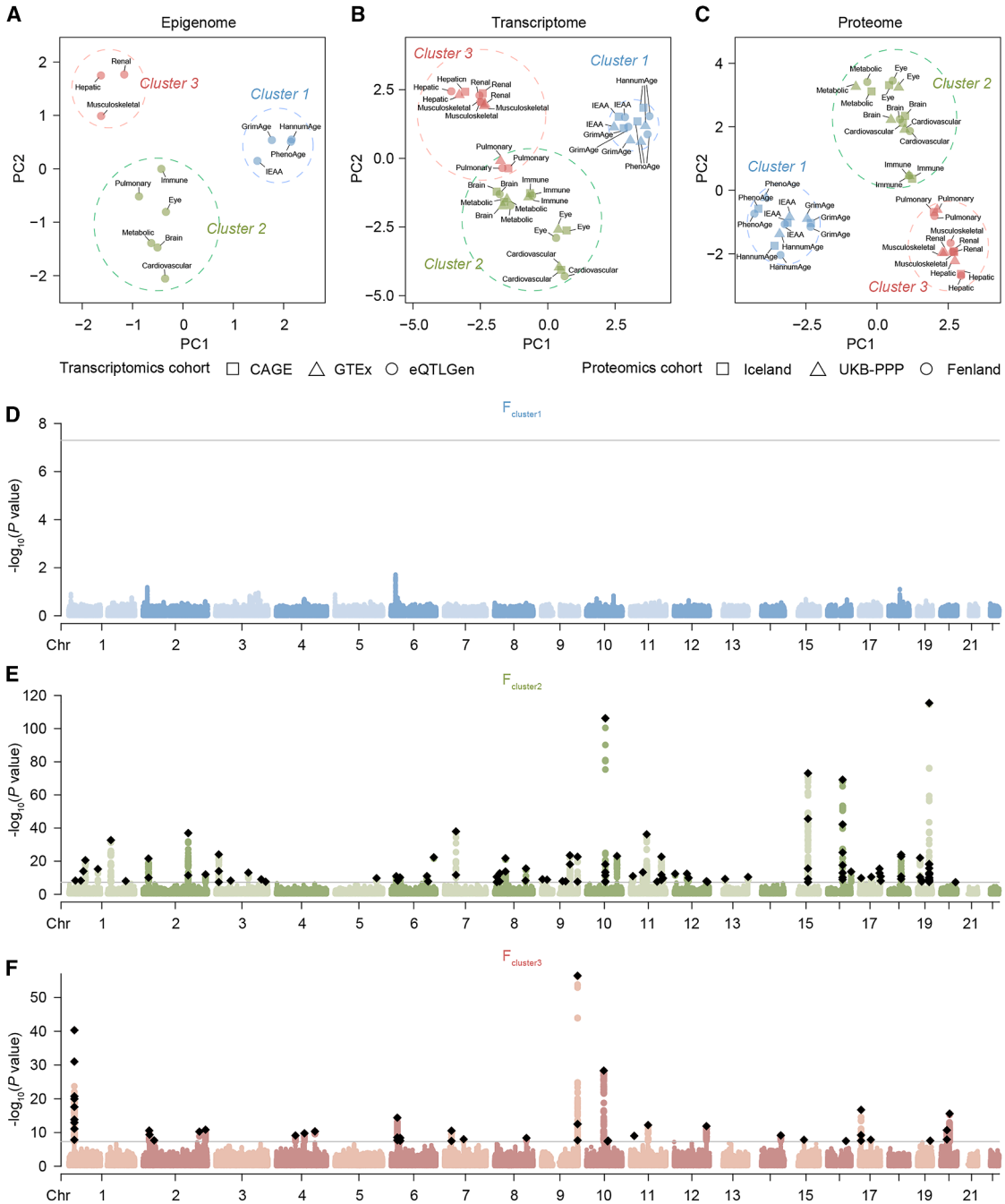

Figure 4. Phenotypic cluster distribution and genetic association patterns of heterogeneous aging across multiple organ systems

(A–C) Distribution of heterogeneous aging-associated phenotypic clusters at epigenomic (A), transcriptomic (B), and proteomic (C) levels.

(D–F) Manhattan plots showing SNP-specific effects on each factor. Black rhombi represent lead SNPs, and a solid line indicates the genome-wide significant threshold ($p = 5 \times 10^{-8}$).

protein in plasma, which in turn promoted genetic susceptibility to cardiovascular aging. Conversely, the remaining 3 sites (cg01934064, cg05772917, and cg23202277) displayed antagonistic regulation, exerting protective regulatory effects on cardiovascular aging susceptibility through suppression of *NMT1* transcription and consequent downregulation of its encoded protein level.

Furthermore, we found that regulatory elements within the same molecular level can influence multiple aging phenotypes through distinct mechanisms. For example, DNAm sites

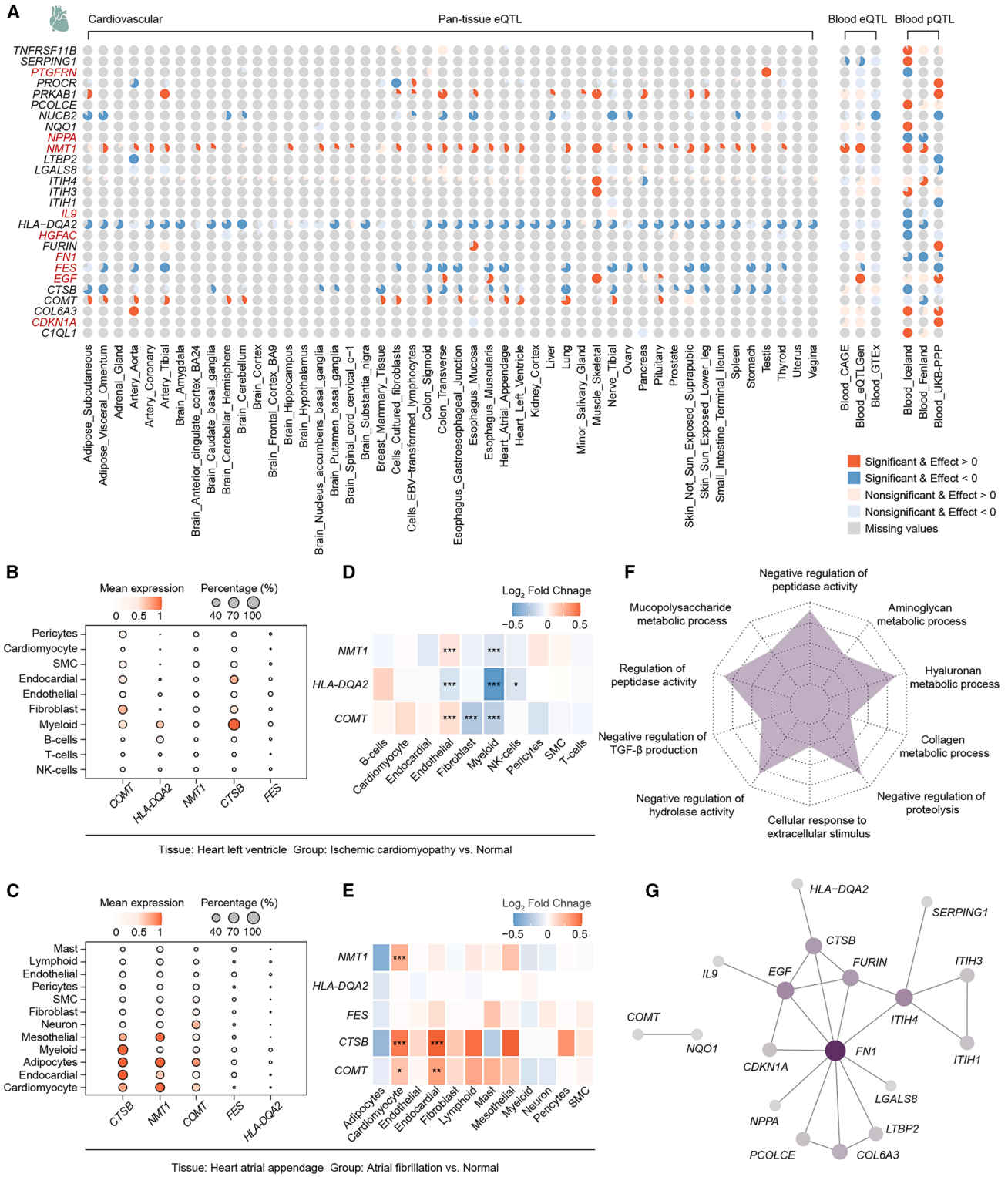

Figure 5. Tissue-specific expression patterns, potential off-target effects, and biological functions of druggable plasma proteins associated with cardiovascular biological age gap

(A) Heatmap showing tissue-specific gene expression effects on cardiovascular biological age gap. Dark red pies represent statistical significance with a positive effect direction, while dark blue pies represent statistical significance with a negative effect direction. The percentage of red and blue in the pie represents the

(legend continued on next page)

cg06961098, cg01656168, cg01762827, and cg06039417 promote genetic susceptibility to epigenetic aging (IEAA), simultaneously affecting organ-specific aging through two separate protein-mediated pathways: decreasing genetic susceptibility to eye aging by downregulating AGRP protein levels while increasing susceptibility to metabolic aging by upregulating LCAT protein levels (Figure S49B). These findings highlight complex regulatory networks connecting epigenetic aging with organ-specific aging, further supporting the concept of biological aging as a multi-dimensional, systemic phenomenon.

Tissue-specific expression patterns and potential off-target effects of candidate druggable plasma proteins

Proteins, as the ultimate executors of gene expression and preferred therapeutic targets, are crucial for advancing tissue-targeted nucleic acid therapies by revealing their tissue-specific expression profiles and potential off-target effects. To understand how identified druggable plasma proteins function through tissue-specific gene regulation, we leveraged eQTL data from 48 tissues in the GTEx project to assess pan-tissue effects on blood-based epigenetic age acceleration and organ-specific biological age gap. Most candidate proteins showed significant concordant directional effects at the transcriptomic and proteomic levels when integrated with peripheral blood data (Figures S50–S53; Table S10). However, there were some exceptions to this general pattern. For instance, while plasma TIE1 protein showed discordant effects on brain biological age gap compared to its peripheral blood transcriptomic effect, its transcriptomic effects in multiple non-blood tissues aligned with the protein effect (Figure S50). This suggests that *TIE1* expression products from non-blood tissues may enter the circulation via secretory pathways and subsequently inhibit brain aging, distinguishing potential on-target and off-target effects of *TIE1*-directed therapies. Overall, the pan-tissue framework effectively parsed expected therapeutic effects from potential non-specific actions across tissues, providing a theoretical foundation for developing therapeutic nucleic acids, including antisense oligonucleotides and small interfering RNAs.

The pan-tissue effect analysis also provides localization guidance for identifying cellular expression of genes encoding proteins associated with blood-based epigenetic age acceleration and organ-specific biological age gap. Among proteins implicated in cardiovascular aging, *NMT1*, *HLA-DQA2*, *FES*, *CTSB*, and *COMT* were predominantly expressed in atrial appendage tissue (Figure 5A). *NMT1*, *HLA-DQA2*, and *COMT* were also expressed in the left ventricle, showing similar associations with cardiovascular aging (Figure 5A). Single-cell and single-nucleus RNA sequencing of the left ventricle and atrial appendage revealed tissue-specific expression patterns of these genes across diverse cell types (Figures 5B, 5C, S53C, and S53D). Furthermore, these genes exhibited differential expression profiles in age-dependent cardiac pathologies, such as ischemic heart disease and atrial fibrillation (Figures 5D, 5E, S53C, and S53D). To elucidate the potential biological effects mediated by these cardiovascular biological age gap-related proteins, we performed functional enrichment and protein-protein interaction network analyses. The results revealed that these proteins, primarily centered around fibronectin encoded by *FN1*, a key extracellular matrix glycoprotein, participate in multiple biological processes closely related to the extracellular matrix, including enzyme activity regulation, mucopolysaccharide metabolism, collagen metabolism, hyaluronic acid metabolism, and aminoglycan metabolism (Figures 5F and 5G).

Phenome-wide association studies elucidate pleiotropic effects of candidate druggable plasma proteins

Aging-related traits manifest across multiple biological scales, encompassing blood-based epigenetic age acceleration and organ-specific biological age gap at the organ level and multivariate longevity phenotypes at the organismal level. To investigate potential associations between candidate druggable plasma proteins linked to organ-level phenotypes and these organismal-level phenotypes, we conducted causal inference analyses across multiple aging-related traits spanning various temporal scales: early-life traits (healthspan, healthy aging, perceived age), mid-to-late-life traits (lifespan, longevity, frailty index, overall health rating), and genetically independent aging traits (Aging-GIP1 and Aging-GIP1-adj), capturing both length of life and indices of mental and physical well-being.[23–28] Among the candidate proteins, 24 demonstrated significant causal relationships with multivariate longevity phenotypes (Figure S54; Table S11). With the exception of PGF protein, which exhibited heterogeneous effects, these proteins consistently demonstrated either pro-longevity or anti-longevity effects. For example, elevated levels of PCSK9 protein were associated with reduced Aging-GIP1, Aging-GIP1-adj, healthy aging, and lifespan, indicating longevity inhibition. Conversely, increased levels of FES protein were associated with extended lifespan, demonstrating longevity promotion.

To model potential effects of pharmacologically targeting candidate druggable plasma proteins, we conducted phenome-wide association studies (PheWASs) using UKB-SAIGE (discovery cohort) and FinnGen (replication cohort) data

effect size. A completely gray pie represents the absence of effective eQTLs for the gene in the corresponding tissue. Genes highlighted in red were supported by evidence from colocalization analysis (PP-H4 > 0.8).

(B) Dot plot showing the average expression levels of selected genes across left ventricle cell types.

(C) Dot plot showing the average expression levels of selected genes across left atrial appendage cell types.

(D) Heatmap showing differential expression of left-ventricle-specific genes across different states (ischemic cardiomyopathy vs. normal). Asterisks represent FDR-adjusted *p* value thresholds: *FDR < 0.05, **FDR < 0.01, and ***FDR < 0.001.

(E) Heatmap showing the differential expression of left-atrial-appendage-specific genes across different states (atrial fibrillation vs. normal). Asterisks represent FDR-adjusted *p* value thresholds: *FDR < 0.05, **FDR < 0.01, and ***FDR < 0.001.

(F) Radar plot showing the biological functions and pathways mediated by druggable plasma proteins associated with cardiovascular biological age gap.

(G) StringDB protein-protein interaction network of druggable plasma proteins associated with cardiovascular biological age gap.

(Table S12). In UKB-SAIGE, the protein encoded by *HLA-DQA2* showed the broadest phenotypic influence, with 23 trait associations, while hypercholesterolemia was associated with 8 proteins, the most among all traits, suggesting susceptibility to multiple protein-mediated effects (Figure S55; Table S12). PCSK9, a well-established target in cardiovascular disease, corroborates the reliability of our PheWAS findings.[29] Elevated plasma PCSK9 levels were strongly associated with increased genetic susceptibility to multiple cardiovascular diseases, including angina pectoris, coronary atherosclerosis, dyslipidemia, hypercholesterolemia, hyperlipidemia, ischemic heart disease, myocardial infarction, and other chronic ischemic heart diseases (Figure S56A; Table S12). Notably, FES protein was negatively correlated with cardiovascular biological age gap, and elevated plasma levels corresponded to reduced genetic susceptibility to these cardiovascular conditions plus hypertension (Figures 2B and S56B; Table S12). In FinnGen, the majority of the findings were validated (Figures S56C and S56D; Table S12). Collectively, with PCSK9 serving as a positive control, these results provide robust evidence supporting FES as a potential cardioprotective target.

Plasma metabolomic effects on heterogeneous aging-related traits

To elucidate plasma metabolite effects on blood-based epigenetic age acceleration and organ-specific biological age gap, we conducted a metabolome-wide Mendelian randomization (MR) analysis of 283 representative plasma metabolites against these aging-related phenotypes. Each metabolite had more than three independent instrumental variables, ensuring adequate statistical power for sensitivity analyses. Using the inverse variance weighted (IVW) method, we identified 2, 16, 28, 19, 20, 17, 6, and 1 metabolites significantly associated with brain, hepatic, immune, metabolic, musculoskeletal, pulmonary, and renal biological age gaps and with PhenoAge, respectively (Table S13). Complementary MR methods validated these associations, with sensitivity analyses confirming directionality and showing no horizontal pleiotropy (Table S13). Figures 6A–6H present the top 5 most significantly positively and negatively correlated metabolites for each phenotype, with complete results available in Table S13.

Given potential multicollinearity from high genetic correlations among metabolites, we further conducted multivariable MR (MVMR) analysis on the significant metabolites identified in the univariate MR analysis to determine genuine causal signals. MVMR identified 2, 2, 8, 2, 5, 5, and 3 metabolites significantly associated with the aforementioned phenotypes (Figure 6I; Table S14). Among these, 25 were phenotype specific, while methionine sulfone positively correlated with both immune and pulmonary biological age gaps, suggesting multi-target anti-aging potential.

Causal protein-metabolite crosstalk networks reveal signal flow across multiple organ systems in heterogeneous aging

To further elucidate the molecular mechanisms linking heterogeneous aging-associated metabolites to multi-omics regulation, we constructed interaction networks connecting these metabolites with upstream epigenomic and transcriptomic regulators and downstream proteomic effectors. This interactive network visualization is available at https://aging-apps.shinyapps.io/heterogeneous-aging/. As protein-metabolite interactions represent fundamental biological regulatory mechanisms, we employed the causal network between circulating proteins and plasma metabolites as a paradigmatic example to unveil this complex bidirectional relationship. Integrated analysis identified 52 significant causal associations involving 27 proteins and 19 metabolites, forming a highly interconnected regulatory network (Figure 6J).

Among the top findings, PCSK9 emerged as a central regulator of heterogeneous aging (Figure 6J). This protein directly promotes genetic susceptibility to metabolic aging while orchestrating heterogeneous aging across multiple organ systems. Specifically, 16α-hydroxy DHEA 3-sulfate negatively correlated with genetic susceptibility to pulmonary aging and potentially inhibited PCSK9 protein abundance. Conversely, PCSK9 upregulated the levels of various lipid metabolites, including lactosyl-N-nervonoyl-sphingosine (d18:1/24:1), palmitoyl dihydrosphingomyelin (d18:0/16:0), stearoyl sphingomyelin (d18:1/18:0), and glutarylcarnitine (C5-DC). These lipids were subsequently associated with genetic susceptibility to immune, metabolic, and renal biological age gaps and further influenced hepatic, metabolic, and pulmonary aging progression through the regulation of downstream circulating proteins. These putative causal networks revealed potential biological pathways, suggesting that aging signals may cascade along these pathways, ultimately leading to heterogeneous aging across multiple organ systems.

Integrative analysis uncovers downstream proteomic and metabolomic effects and detectable biomarkers of heterogeneous aging

We identified potential druggable plasma proteins and metabolites associated with blood-based epigenetic age acceleration and organ-specific biological age gap. However, the downstream molecular perturbations mediated by these heterogeneous aging-related traits and the readily detectable biomarkers characterizing the progression of these aging processes remain to be elucidated.

To address this gap, we extracted genetic variants associated with these aging-related traits and implemented proteome-wide MR using plasma protein data from Iceland, Fenland, and UKB-PPP to elucidate variant effects on the plasma proteome (Table S15). At an FDR threshold of 0.05, metabolic, hepatic, and renal biological age gaps induced more extensive downstream protein perturbations than musculoskeletal, pulmonary, and immune age gaps and GrimAge (Figures 7A and S57). Functional enrichment analysis demonstrated that metabolic biological age gap primarily influenced cholesterol, lipoprotein, and fatty acid metabolism, as well as complement and coagulation-related biological processes (Figure 7B). Hepatic biological age gap appeared to induce significant perturbations in other organs, such as the kidney, vasculature, and bones (Figure 7C). Renal biological age gap drove extensive modulations in inflammatory and immune biological processes, encompassing leukocyte-mediated immunity, canonical NF-κB signal transduction, interleukin-1 production, chemokine production, and regulation

CellPress
OPEN ACCESS

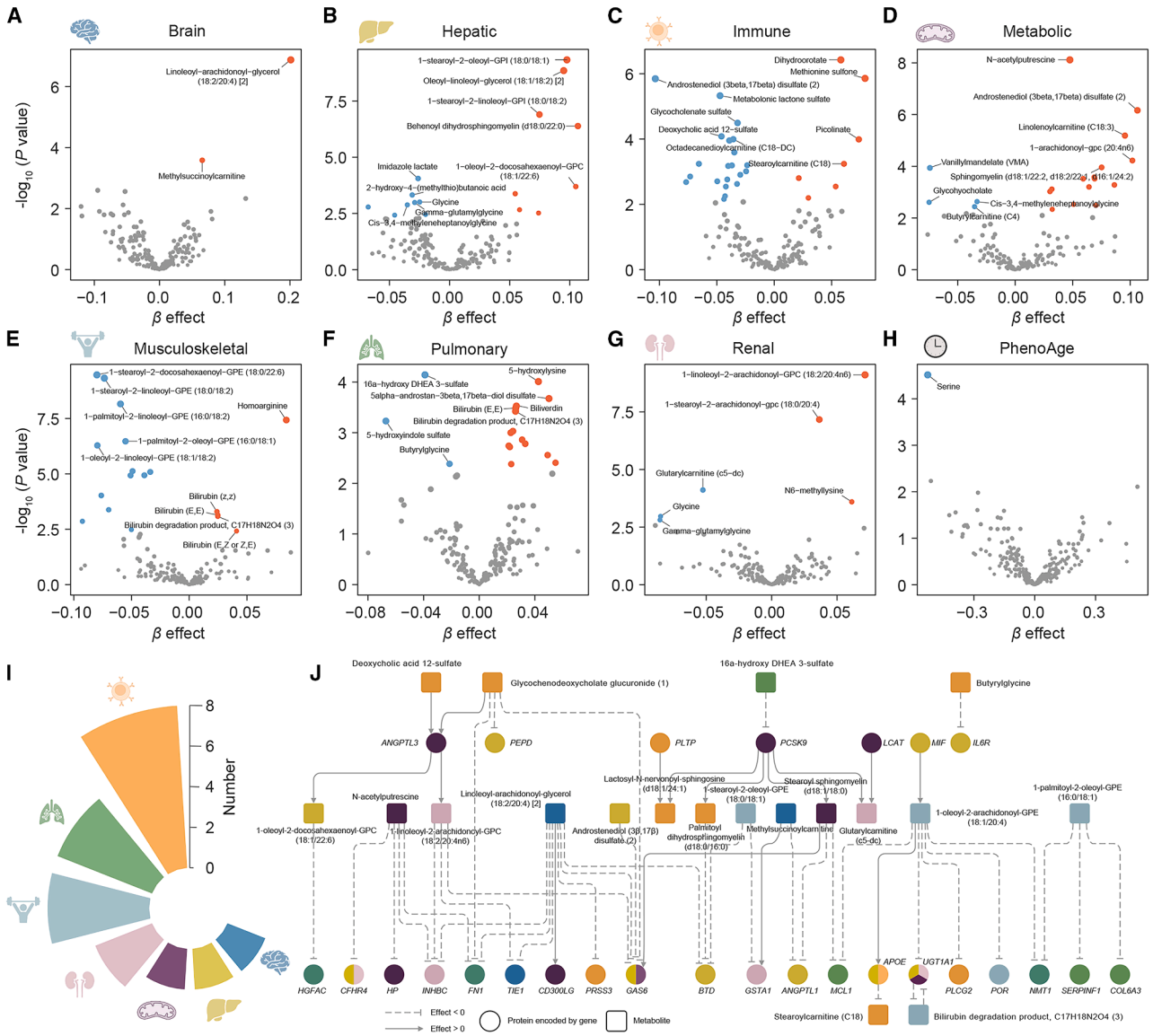

Figure 6. Plasma metabolites associated with heterogeneous aging-related phenotypes and their protein-metabolite causal crosstalk networks

(A–H) Volcano plots showing the effects of plasma metabolites on organ-specific biological age gap and blood-based epigenetic age acceleration. The five most significantly positively correlated and five most significantly negatively correlated metabolites (FDR < 0.05) are labeled, with the complete results included in Table S13.

(I) Nightingale rose chart showing the number of significant metabolites (FDR < 0.05) associated with each aging-related trait after MVMR analysis.

(J) Protein-metabolite causal crosstalk networks orchestrating heterogeneous aging across multiple organ systems. Each geometric shape represents a specific molecular type, while each color denotes candidate causal targets specific to the corresponding organ system.

of inflammatory responses (Figure 7D). These findings suggest that organ aging is not an isolated phenomenon, and its downstream effects may have far-reaching consequences on other organs. To explore potential inter-organ interactions, we integrated the druggable plasma proteins identified for each organ to determine whether aging in one organ accelerates the biological age gap in others. This revealed an intricate interaction network between organ systems (Figure 7E). For instance, hepatic biological age gap negatively correlated with HGFAC protein, which in turn negatively correlated with cardiovascular biological age gap. This hepatic-HGFAC-cardiovascular axis suggests that hepatic aging may accelerate cardiovascular aging through reduced HGFAC protein levels, reflecting the mutual communication between hepatic and cardiovascular system.

Metabolome-wide MR analysis of genetic variant impacts on 861 plasma metabolites revealed that, at FDR < 0.05, metabolic, renal, musculoskeletal, and immune biological age gaps induce significant downstream metabolic perturbations, with the

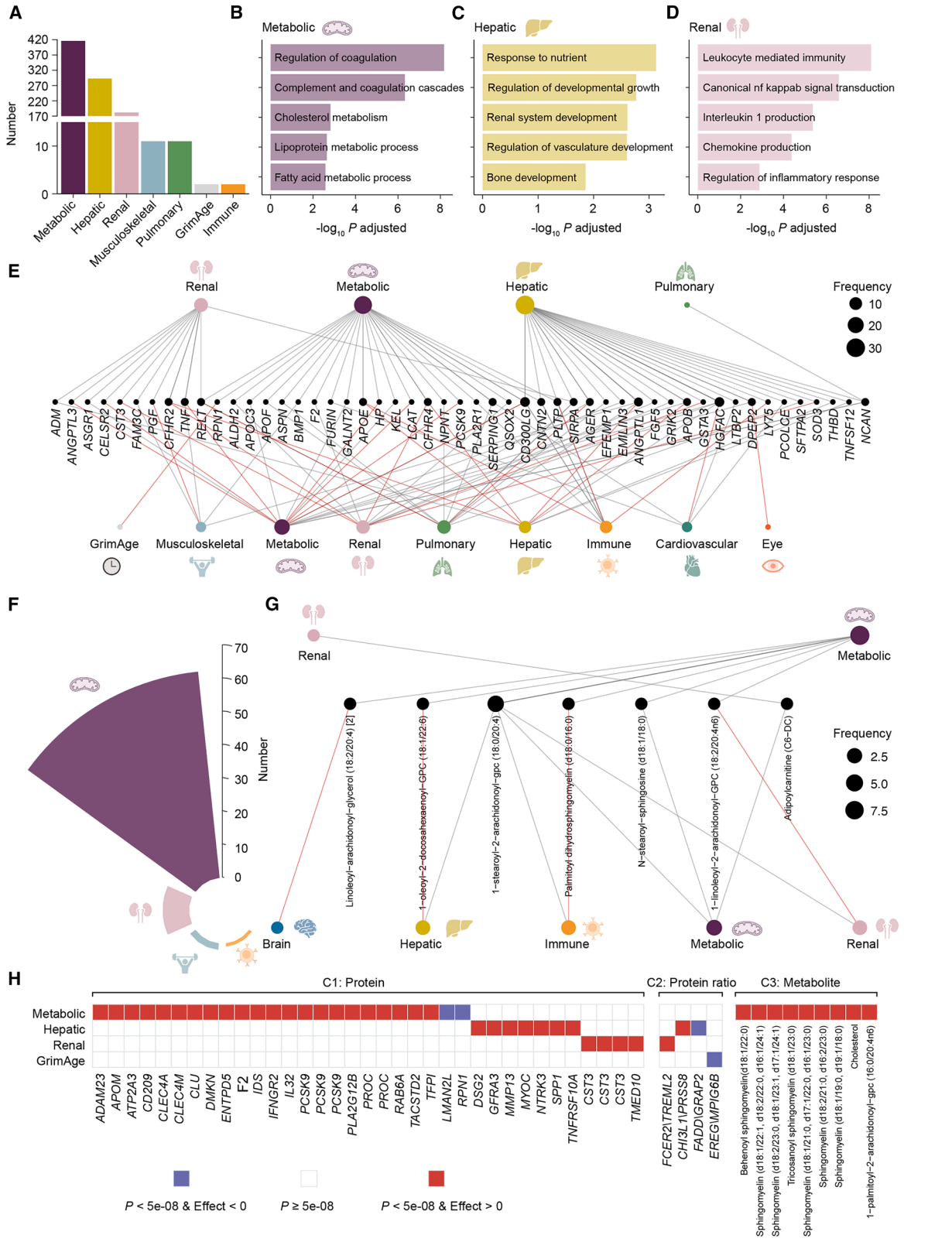

(legend on next page)

metabolic biological age gap showing the strongest effects (Figures 7F and S58; Table S16). Integrated analysis further indicated that plasma metabolites, similar to circulating proteins, play an important intermediary role in the crosstalk between organ-specific biological age gaps (Figure 7G).

To identify readily detectable biomarkers representing heterogeneous aging, we applied a stringent genome-wide significance threshold of 5×10^{-8}, although this conservative threshold may yield false negatives. Additionally, considering the clinical relevance of protein ratios, we incorporated ratios between protein levels (rQTL) data analysis of plasma proteins (Table S17). For metabolic biological age gap, we identified 21 unique proteins and 9 metabolites; for hepatic biological age gap, 7 unique proteins and 2 protein ratios; for renal biological age gap, 2 unique proteins and 1 protein ratio; and for blood-based epigenetic age acceleration (GrimAge), 1 protein ratio (Figure 7H). Notably, cystatin-C (*CST3*), a well-established renal injury biomarker, was validated across three independent datasets, confirming analytical reliability and robustness. These biomarkers may facilitate preclinical testing to assess the degree of organ-specific aging in individuals.

Systematic evaluation of candidate druggable plasma proteins and development of an interactive web tool

To further advance research on drug targets for heterogeneous aging across multiple organ systems, we systematically summarized the druggable plasma proteins identified in this study. These proteins can be categorized into two groups: candidate targets with suggestive significance (FDR_SMR < 0.05 and p_HEIDI > 0.05 and PP-H4 < 0.8) and key targets with colocalization evidence (FDR_SMR < 0.05 and p_HEIDI > 0.05 and PP-H4 > 0.8) (Table S18). For key targets, we conducted a comprehensive evaluation from multiple dimensions, including age-related changes from longitudinal observational studies, drug development feasibility ratings, target safety assessments, epigenetic regulation, transcriptional regulation, metabolic regulation, pan-tissue effects of targets, multivariate longevity phenotype association effects, and multi-organ aging interaction network node analysis. Additionally, we developed an interactive visualization web tool (https://aging-apps.shinyapps.io/heterogeneous-aging/) enabling exploration of potential causal molecular targets and biomarkers for heterogeneous aging-related phenotypes and their downstream biological effects at more flexible statistical thresholds beyond the FDR < 0.05 used here. More importantly, this resource incorporates dynamic interactive visualization functionality for cross-level causal inference networks underlying heterogeneous aging across multiple organ systems, guided by the central dogma of molecular biology. By displaying hierarchical regulatory relationships and interaction patterns across multi-omics data, this tool holds particular value for understanding the biological aging mechanisms across multiple organ systems and potentially accelerating the identification and development of drug targets for future interventions.

DISCUSSION

Our study employed large-scale genomic data to investigate the global and local genetic correlations between epigenetic age acceleration assessed by four established blood-based epigenetic clocks and biological age gap quantified by nine recently developed organ-specific aging clocks. Using an integrative multi-omics analysis combining proteomics, transcriptomics, and epigenomics, we identified three distinct phenotypic clusters of heterogeneous aging, prioritized genetic drug targets, and mapped cross-layer regulatory networks linking the epigenome, transcriptome, and proteome. By integrating association signals from 48 GTEx tissues, we systematically evaluated the cross-tissue on-target and off-target effects of these targets. PheWAS further delineated their beneficial effects (potential repurposing opportunities) and unintended effects (possible adverse reactions) on multivariate longevity phenotypes and comprehensive binary traits. We also highlighted plasma metabolites that modulate blood-based epigenetic age acceleration and organ-specific biological age gap, revealing protein-metabolite causal networks orchestrating multiple organ system heterogeneous aging cascades. The statistically significant signals identified across all omics layers represent priority pharmacological targets for personalized anti-aging strategies. Furthermore, MR analyses uncovered downstream proteomic and metabolomic effects mediated by heterogeneous aging, identifying detectable biomarkers that characterize aging in specific organs and systems. Integrating these downstream biological effects with potential pharmacological targets further elucidated mechanisms of whole-body, multi-organ aging interactions. These findings provide a comprehensive molecular landscape revealing multi-omic underpinnings of heterogeneous aging, with implications for basic research and translational efforts to extend healthspan.

Despite the significant clinical usefulness of epigenetic clocks and their important insights into aging biology across tissue types, emerging evidence indicates that aging varies markedly between organ systems.[2] However, the phenotypic relationship

Figure 7. Downstream effects and detectable biomarkers of heterogeneous aging

(A) Bar plot showing the number of significant downstream plasma protein perturbations (FDR < 0.05) across heterogeneous aging-related phenotypes.

(B–D) Functional enrichment analysis of downstream plasma protein perturbations caused by metabolic (B), hepatic (C), and renal (D) aging.

(E) Interaction network of organ aging mediated by druggable plasma proteins. The protein-coding genes with red connecting lines have supporting evidence of colocalization (PP-H4 > 0.8).

(F) Nightingale rose chart showing the number of significant downstream plasma metabolite perturbations (FDR < 0.05) across heterogeneous aging-related phenotypes.

(G) Interaction network of organ aging mediated by plasma metabolites. The metabolites with red connecting lines have supporting evidence of colocalization (PP-H4 > 0.8).

(H) Heatmap showing significant detectable plasma biomarkers ($p < 5 \times 10^{-8}$) associated with heterogeneous aging-related phenotypes, including proteins, protein-to-protein ratios, and metabolites.

between organ-specific aging and blood-based epigenetic aging remains unclear. Drawing on Cheverud's conjecture, genetic correlation can serve as a surrogate for phenotypic correlation.[30] We conducted global and local genetic correlation analyses between these two types of aging patterns. The results reveal complex genetic associations between blood-based epigenetic aging and organ-specific aging, exhibiting both homogeneity and heterogeneity.

Through integrated multi-omics clustering analysis incorporating epigenomics, transcriptomics, and proteomics, we further categorized these heterogeneous aging characteristics into three distinct phenotypic clusters. These clusters showed remarkably consistent classification patterns across multiple regulatory levels, exhibiting significant cross-molecular-layer homogeneity and conservation. Notably, pulmonary aging displayed unique molecular dynamics, with the aging signature demonstrating a progressive transition along the central dogma cascade from epigenome through transcriptome to proteome—gradually shifting from cluster 2 to cluster 3. This cross-molecular phenotypic plasticity may capture the temporal evolution of the pulmonary aging process, whereby early epigenetic alterations propagate through intermediate transcriptional states to ultimately establish stable proteomic signatures. This phenomenon likely reflects adaptive regulatory mechanisms that emerge in response to continuous and variable environmental exposures in the lung.[31] Furthermore, functional enrichment analysis of these clusters further revealed cluster-specific biological characteristics while also demonstrating the convergence of heterogeneous aging-associated phenotypes in their shared biological hallmarks, such as response to stimulus, inflammatory response, and immune cell development and activation. The extensive activation of immune cells is unequivocally associated with chronic inflammation, which aligns with previous studies supporting that inflammation fuels aging at the systemic level[32,33] and further extends this finding, indicating that various hyperactivated immune cells accumulating in diverse organs represent a prominent organ-specific inflammaging characteristic. Subsequently, a multivariate GWAS systematically elucidated the genetic basis underlying distinct phenotypic clusters, identifying the potential common genetic regulatory factors and characterizing functional variants, DNAm sites, druggable genes, and circulating proteins associated with these factors. Collectively, these findings provide preliminary biological insights for reexamining the boundaries and subtypes of multi-organ system heterogeneous aging from a molecular signature perspective.

Age-related chronic diseases represent accelerated aging of their respective biological systems or subsystems, the epitome of accelerated organ- and system-specific aging.[2,34] Connecting molecular signature- and biological function-associated multi-organ system heterogeneous aging phenotypes and dissecting their shared genetic architecture could help explain why seemingly unrelated chronic diseases occur simultaneously in patients and further aid in mechanistic understanding and effective therapeutics from a systems biology perspective. Furthermore, these findings highlight the complementary value of organ-specific aging clocks to existing blood-based epigenetic clocks in characterizing aging heterogeneity. Future research could develop cluster-specific polygenic risk scores based on heterogeneous aging-related features to achieve more precise quantitative assessment of individual aging status.

Plasma proteomics-based biological aging clocks suggest that circulating proteins may serve as therapeutic targets for anti-aging interventions.[35,36] However, associations between protein levels and biological aging from cross-sectional observational studies make it challenging to establish definitive causal evidence. While randomized controlled trials (RCTs) represent the gold standard for evaluating causality, conducting RCTs with protein levels as intervention factors might be neither feasible nor ethical. MR leverages natural genetic variations to simulate RCTs for establishing causality in non-randomized studies.[37] Since genetic variants are randomly allocated at conception, causal effects estimated through MR help circumvent confounding by factors such as environmental exposures and lifestyle factors.[38] Based on this principle, we integrated pQTL data from multiple cohorts within an MR framework to identify plasma proteins potentially causally associated with heterogeneous aging across multiple organ systems, following current methodological recommendations from large-scale plasma proteomics comparisons.[39] Considering that genetically proximal traits are less susceptible to horizontal pleiotropy than complex traits with a polygenic genetic architecture,[11] we extended this strategy to epigenomic, transcriptomic, and metabolomic levels, constructing a multi-omics causal regulatory network underlying heterogeneous aging. In this network, we summarized three predominant regulatory modes.

The first regulatory mode involves hierarchical control within molecular networks. It encompasses vertical regulation along the epigenetic-transcriptional-protein axis and horizontal coordination among functional pathways composed of circulating proteins and plasma metabolites, with both dimensions showing synergistic and antagonistic effects. The second mode comprises bidirectional networks connecting epigenetic aging and organ-specific aging. The third mode forms a cascade signaling axis that establishes temporal aging sequences, where aging in one organ triggers heterogeneous aging of downstream organs through specific plasma proteins or metabolites, contrasting with the synchronous multi-organ system regulation observed in the first two modes.

The regulatory network of heterogeneous aging across multiple organ systems suggests that system-level aging unfolds through a series of dynamic changes in organ-specific aging. Accelerated-aging organs exert "gravitational effects" that place other organs in varying aging states, which are compensated through interactions with relatively younger organs within the organism, although such compensation may progressively diminish as "entropy increases" during systemic aging progression. Furthermore, this systemic transmission of organ-specific aging correlates with various pathological conditions. Previous studies have demonstrated that comprehensive organ aging increases mortality risk, while individual organ aging predicts the development of organ-specific age-related diseases.[2,36] For example, subjects with accelerated brain or vascular aging exhibit higher incidence rates of Alzheimer's disease, while those with accelerated heart aging show significantly elevated risks of heart failure. *HGFAC*, encoding hepatocyte growth factor activator serine protease, has recently been identified as a

candidate mediator in liver-heart communication involved in heart failure,[40] confirming the role of the hepatic-HGFAC-cardiovascular biological age gap axis in regulating multi-organ aging and age-related chronic disease onset. Consequently, we provide a unique resource that establishes a crucial hypothesis-generating foundation for further experimental investigations by offering contextual information regarding potential mechanisms underlying heterogeneous aging across multiple organ systems and associated chronic diseases.

Genetically supported causal relationships can significantly increase the probability of therapeutic success in phase III trials and subsequent marketing approval.[41,42] Our hypothesis-free, genetics-driven analytical paradigm provides hypothesis generation for exploring interventions that could halt or even reverse organ-specific aging. Using PCSK9 as a validation, longitudinal observational studies have demonstrated that its plasma levels increase with age,[36] exhibiting the highest druggability (tier 1) and safety ratings (safety scale of 1). Our research indicated that PCSK9 concentrations correlate with increased genetic susceptibility to metabolic aging, consistent with its expected role in lipid metabolism,[29] suggesting its therapeutic potential for metabolic aging intervention. Multivariate longevity phenotype analysis revealed negative correlations between PCSK9 and early-life aging trait (healthy aging), mid-to-late-life aging trait (lifespan), and genetically independent aging phenotypes (Aging-GIP1 and Aging-GIP1-adj), further supporting its potential application as a systemic anti-aging target.

The *FES* gene encodes the tyrosine protein kinase Fes/Fps, which regulates multiple cellular functions, including cell motility, proliferation, differentiation, survival, and inflammation.[43,44] We found that circulating FES protein levels negatively correlate with genetic susceptibility to cardiovascular aging, and multivariate longevity phenotype analysis linked higher levels to increased lifespan. *FES* exhibits a druggability tier of 2 and a safety scale of 4, suggesting its translational potential for anti-cardiovascular aging interventions. Notably, PheWAS analysis further indicated its association with reduced genetic susceptibility to various cardiovascular chronic diseases, including coronary atherosclerosis. A recent animal model study demonstrated that *Fes* knockout increases atherosclerotic plaque size in apolipoprotein E-deficient mice on high-fat diets, although the specific mechanism remains unclear.[45] Combined with our findings, the anti-cardiovascular aging effects mediated by *FES* may represent one of the crucial mechanisms underlying its cardiovascular protective function.

In addition to identifying priority drug targets for heterogeneous aging across multiple organ systems, we integrated multi-omics data and employed a more stringent genome-wide significance threshold (5×10^{-8}) to define potential biomarkers for organ-specific aging and blood-based epigenetic aging. For instance, genetically predicted renal aging was associated with elevated circulating CST3 protein levels, consistent with the established clinical use of cystatin-C as a renal dysfunction indicator,[46] thereby validating the robustness of our approach. Osteopontin (*SPP1*), recently described as a robust serum biomarker in patients with non-alcoholic steatohepatitis, has been linked to the progression of liver fibrosis.[47,48] We further extended this finding by demonstrating that osteopontin could serve as a downstream detectable biomarker for accelerated hepatic biological aging. Notably, these significant signatures may also function as biomarkers for drug responses targeting upstream organ-specific aging and blood-based epigenetic aging, informing future anti-aging therapeutics.

In conclusion, using hypothesis-free, genetically driven statistical approaches, we present a paradigm for integrating multi-layered omics data (genomics, epigenomics, transcriptomics, proteomics, and metabolomics). This systems biology framework revealed convergence and heterogeneity between organ-specific aging and blood-based epigenetic aging while elucidating molecular signatures of multi-organ systemic aging, providing crucial hypothesis-generating foundations for deciphering the regulatory networks underlying heterogeneous aging across multiple organ systems. Further experimental investigations based on these hypotheses are needed to explore specific mechanisms involved. Since we could discuss only a fraction of the biological findings, we developed an interactive visualization R/Shiny application (https://aging-apps.shinyapps.io/heterogeneous-aging/) for data sharing and exploration. This open-access resource will enable the research community to gain deeper insights into the mechanisms of heterogeneous aging across multiple organ systems and accelerate the development of aging biomarkers and therapeutic targets.

Limitations of the study

Several limitations warrant discussion when interpreting our results. First, potential drug targets identified from multi-omics data may not all successfully translate into clinical therapeutics. Our prioritization aims to narrow the target scope to optimize resource allocation and reduce risks in development time and cost, which is the primary focus of this study. These findings therefore should be viewed as hypothesis-generating foundations requiring systematic experimental validation to elucidate the more specific regulatory mechanisms underlying multiple organ system heterogeneous aging. Second, following current recommendations from large-scale plasma proteomics comparisons,[39] we leveraged orthogonal evidence across technological platforms using independent proteomics data from UKB-PPP, Iceland, and Fenland cohorts, thereby minimizing potential biases associated with reliance on a single platform or data source. While integrating multiple cohorts may introduce potential population heterogeneity, this effect is likely minimal given the statistical advantages of post-GWAS methodologies and the consistency of clustering results observed across cohorts. Third, although genetically proximal molecular phenotypes are less susceptible to horizontal pleiotropy compared to complex traits with polygenic architecture,[11] the causal relationships identified in our study should be interpreted cautiously given MR assumptions. Furthermore, our multi-omic regulatory network analysis did not incorporate mechanisms regulating coding gene expression beyond DNAm, such as non-coding RNA-mediated transcriptional regulation. As additional multi-omic genetic data become available, we anticipate these insights will be further refined and expanded. Fourth, MR analyses of drug targets may be more suitable as a reliable verification for the direction of effect, as drugs usually work by modifying target function rather than concentration. MR estimates are thought to

reflect lifelong exposure, but in the absence of serial assessments, they are unable to consider the time-varying effects. Thus, we suggest that drug target MR provides a robust directional guidance but may not directly predict pharmacological intervention effect sizes. Based on these insights, we position our findings as a valuable resource to guide ongoing and future drug trials.[42] Future work could be advanced in two directions: (1) through longitudinal study designs to thoroughly investigate the time/age-dependent effects of genetic variants and (2) by developing novel causal organ-specific aging clocks based on the causal relationships inferred from our study, analogous to the recently constructed next-generation causality-enriched damage and adaptation epigenetic clocks using MR methodology.[49] Fifth, the scarcity of multi-omics datasets limited our analyses to European populations, restricting the generalizability of the research findings to other populations. Once more comprehensive genetic data are generated in the future, our pipeline should be conducted in non-European-ancestry populations to prevent the perpetuation of health disparities arising from limited generalizability.

RESOURCE AVAILABILITY

Lead contact

Requests for further information and resources should be directed to and will be fulfilled by the lead contact, Yingfeng Tu (tyfdoctor@hrbmu.edu.cn).

Materials availability

This study did not generate new, unique reagents.

Data and code availability

All data used in this study and the corresponding access information are listed in the key resources table. The summary statistics for multivariate GWAS of $F_{cluster1}$, $F_{cluster2}$, and $F_{cluster3}$ generated in this study are publicly available at https://aging-apps.shinyapps.io/heterogeneous-aging. This study did not generate any unique code. Links to the public software and algorithms used in the present study are listed in the key resources table. The interactive visualization web tool of heterogeneous aging that we developed is publicly available at https://aging-apps.shinyapps.io/heterogeneous-aging.

ACKNOWLEDGMENTS

This work was supported by the National Natural Science Foundation of China (81871402 to Y.T.), the Scientific Research Foundation for Postdoctoral Heilongjiang Province of China (LBH-Q19037 to Y.T.), and the Doctoral Start-up Fund of Yangzhou University (2024BS-LZY to Z.L.). We thank all the participants of the GWASs used in this study and the researchers who made the GWAS data publicly available. We are also grateful to the authors and participants of the studies cited in this work, and we acknowledge the Wen laboratory (https://labs-laboratory.com/) and Yang laboratory (https://yanglab.westlake.edu.cn/) for sharing data and software. Without them, this work would not have been possible. Selected elements in the graphical abstract, Figures 1 and 2, and all organ images were created with BioRender (https://www.biorender.com/).

AUTHOR CONTRIBUTIONS

J.X. conceived the idea and designed the study. J.X. performed the analyses and wrote the manuscript. J.X., X.Z., Y.G., H.T., C.D., B.W., M.L., Z.L., and Y.T. critically revised the manuscript for important intellectual content. J.X. and Z.L. created the graphical abstract. Z.L. and Y.T. obtained financial support and supervised the study.

DECLARATION OF INTERESTS

The authors declare no competing interests.

STAR★METHODS

Detailed methods are provided in the online version of this paper and include the following:

- KEY RESOURCES TABLE
- EXPERIMENTAL MODEL AND SUBJECT DETAILS
- METHOD DETAILS
  - Global genetic correlation analysis
  - Local genetic correlation analysis
  - Druggable genome data
  - SMR & HEIDI analysis
  - Colocalization analysis
  - Clustering analysis
  - Gene set enrichment analysis
  - Genomic SEM
  - Q_{SNP} heterogeneity
  - Identification of genomic loci and variants
  - Fine mapping
  - Identification of cross-layer molecular regulatory networks
  - Tissue-specific analysis
  - Multivariate longevity phenotype analysis
  - Phenome-wide association study
  - Metabolome-wide Mendelian randomization
  - Downstream effects mediated by heterogeneous aging
  - Single-cell RNA sequencing and single-nucleus RNA sequencing analyses
  - Functional enrichment analysis
  - Protein-protein interaction network analysis
- QUANTIFICATION AND STATISTICAL ANALYSIS

SUPPLEMENTAL INFORMATION

Supplemental information can be found online at https://doi.org/10.1016/j.xgen.2025.101032.

Received: October 25, 2024
Revised: February 16, 2025
Accepted: September 8, 2025
Published: October 2, 2025

REFERENCES

1. Niccoli, T., and Partridge, L. (2012). Ageing as a risk factor for disease. Curr. Biol. *22*, R741–R752.
2. Tian, Y.E., Cropley, V., Maier, A.B., Lautenschlager, N.T., Breakspear, M., and Zalesky, A. (2023). Heterogeneous aging across multiple organ systems and prediction of chronic disease and mortality. Nat. Med. *29*, 1221–1231.
3. Guarente, L., Sinclair, D.A., and Kroemer, G. (2024). Human trials exploring anti-aging medicines. Cell Metab. *36*, 354–376.
4. Kaeberlein, M., Rabinovitch, P.S., and Martin, G.M. (2015). Healthy aging: The ultimate preventative medicine. Science *350*, 1191–1193.
5. Teschendorff, A.E., and Horvath, S. (2025). Epigenetic ageing clocks: statistical methods and emerging computational challenges. Nat. Rev. Genet. *26*, 350–368.
6. Hannum, G., Guinney, J., Zhao, L., Zhang, L., Hughes, G., Sadda, S., Klotzle, B., Bibikova, M., Fan, J.B., Gao, Y., et al. (2013). Genome-wide methylation profiles reveal quantitative views of human aging rates. Mol. Cell *49*, 359–367.

7. Horvath, S. (2013). DNA methylation age of human tissues and cell types. Genome Biol. *14*, R115.

8. Levine, M.E., Lu, A.T., Quach, A., Chen, B.H., Assimes, T.L., Bandinelli, S., Hou, L., Baccarelli, A.A., Stewart, J.D., Li, Y., et al. (2018). An epigenetic biomarker of aging for lifespan and healthspan. Aging *10*, 573–591.

9. Lu, A.T., Quach, A., Wilson, J.G., Reiner, A.P., Aviv, A., Raj, K., Hou, L., Baccarelli, A.A., Li, Y., Stewart, J.D., et al. (2019). DNA methylation GrimAge strongly predicts lifespan and healthspan. Aging *11*, 303–327.

10. Wen, J., Tian, Y.E., Skampardoni, I., Yang, Z., Cui, Y., Anagnostakis, F., Mamourian, E., Zhao, B., Toga, A.W., Zalesky, A., and Davatzikos, C. (2024). The genetic architecture of biological age in nine human organ systems. Nat. Aging *4*, 1290–1307.

11. Holmes, M.V., Richardson, T.G., Ference, B.A., Davies, N.M., and Davey Smith, G. (2021). Integrating genomics with biomarkers and therapeutic targets to invigorate cardiovascular drug development. Nat. Rev. Cardiol. *18*, 435–453.

12. McRae, A.F., Marioni, R.E., Shah, S., Yang, J., Powell, J.E., Harris, S.E., Gibson, J., Henders, A.K., Bowdler, L., Painter, J.N., et al. (2018). Identification of 55,000 Replicated DNA Methylation QTL. Sci. Rep. *8*, 17605.

13. Lloyd-Jones, L.R., Holloway, A., McRae, A., Yang, J., Small, K., Zhao, J., Zeng, B., Bakshi, A., Metspalu, A., Dermitzakis, M., et al. (2017). The Genetic Architecture of Gene Expression in Peripheral Blood. Am. J. Hum. Genet. *100*, 228–237.

14. Consortium, G.T. (2020). The GTEx Consortium atlas of genetic regulatory effects across human tissues. Science *369*, 1318–1330.

15. Vosa, U., Claringbould, A., Westra, H.J., Bonder, M.J., Deelen, P., Zeng, B., Kirsten, H., Saha, A., Kreuzhuber, R., Yazar, S., et al. (2021). Large-scale cis- and trans-eQTL analyses identify thousands of genetic loci and polygenic scores that regulate blood gene expression. Nat. Genet. *53*, 1300–1310.

16. Ferkingstad, E., Sulem, P., Atlason, B.A., Sveinbjornsson, G., Magnusson, M.I., Styrmisdottir, E.L., Gunnarsdottir, K., Helgason, A., Oddsson, A., Halldorsson, B.V., et al. (2021). Large-scale integration of the plasma proteome with genetics and disease. Nat. Genet. *53*, 1712–1721.

17. Pietzner, M., Wheeler, E., Carrasco-Zanini, J., Cortes, A., Koprulu, M., Wörheide, M.A., Oerton, E., Cook, J., Stewart, I.D., Kerrison, N.D., et al. (2021). Mapping the proteo-genomic convergence of human diseases. Science *374*, eabj1541.

18. Sun, B.B., Chiou, J., Traylor, M., Benner, C., Hsu, Y.H., Richardson, T.G., Surendran, P., Mahajan, A., Robins, C., Vasquez-Grinnell, S.G., et al. (2023). Plasma proteomic associations with genetics and health in the UK Biobank. Nature *622*, 329–338.

19. Wu, Y., Zeng, J., Zhang, F., Zhu, Z., Qi, T., Zheng, Z., Lloyd-Jones, L.R., Marioni, R.E., Martin, N.G., Montgomery, G.W., et al. (2018). Integrative analysis of omics summary data reveals putative mechanisms underlying complex traits. Nat. Commun. *9*, 918.

20. Finan, C., Gaulton, A., Kruger, F.A., Lumbers, R.T., Shah, T., Engmann, J., Galver, L., Kelley, R., Karlsson, A., Santos, R., et al. (2017). The druggable genome and support for target identification and validation in drug development. Sci. Transl. Med. *9*, eaag1166.

21. Zhu, Z., Zhang, F., Hu, H., Bakshi, A., Robinson, M.R., Powell, J.E., Montgomery, G.W., Goddard, M.E., Wray, N.R., Visscher, P.M., and Yang, J. (2016). Integration of summary data from GWAS and eQTL studies predicts complex trait gene targets. Nat. Genet. *48*, 481–487.

22. Oliva, M., Demanelis, K., Lu, Y., Chernoff, M., Jasmine, F., Ahsan, H., Kibriya, M.G., Chen, L.S., and Pierce, B.L. (2023). DNA methylation QTL mapping across diverse human tissues provides molecular links between genetic variation and complex traits. Nat. Genet. *55*, 112–122.

23. Zenin, A., Tsepilov, Y., Sharapov, S., Getmantsev, E., Menshikov, L.I., Fedichev, P.O., and Aulchenko, Y. (2019). Identification of 12 genetic loci associated with human healthspan. Commun. Biol. *2*, 41.

24. Timmers, P.R.H.J., Wilson, J.F., Joshi, P.K., and Deelen, J. (2020). Multivariate genomic scan implicates novel loci and haem metabolism in human ageing. Nat. Commun. *11*, 3570.

25. Roberts, V., Main, B., Timpson, N.J., and Haworth, S. (2020). Genome-Wide Association Study Identifies Genetic Associations with Perceived Age. J. Invest. Dermatol. *140*, 2380–2385.

26. Timmers, P.R., Mounier, N., Lall, K., Fischer, K., Ning, Z., Feng, X., Bretherick, A.D., Clark, D.W., eQTLGen Consortium; and Shen, X., et al. (2019). Genomics of 1 million parent lifespans implicates novel pathways and common diseases and distinguishes survival chances. eLife *8*, e39856.

27. Atkins, J.L., Jylhävä, J., Pedersen, N.L., Magnusson, P.K., Lu, Y., Wang, Y., Hägg, S., Melzer, D., Williams, D.M., and Pilling, L.C. (2021). A genome-wide association study of the frailty index highlights brain pathways in ageing. Aging Cell *20*, e13459.

28. Timmers, P.R.H.J., Tiys, E.S., Sakaue, S., Akiyama, M., Kiiskinen, T.T.J., Zhou, W., Hwang, S.J., Yao, C., et al.; Biobank Japan Project; FinnGen (2022). Mendelian randomization of genetically independent aging phenotypes identifies LPA and VCAM1 as biological targets for human aging. Nat. Aging *2*, 19–30.

29. Preiss, D., Tobert, J.A., Hovingh, G.K., and Reith, C. (2020). Lipid-Modifying Agents, From Statins to PCSK9 Inhibitors: JACC Focus Seminar. J. Am. Coll. Cardiol. *75*, 1945–1955.

30. Cheverud, J.M. (1988). A Comparison of Genetic and Phenotypic Correlations. Evolution *42*, 958–968.

31. Eckhardt, C.M., and Wu, H. (2021). Environmental Exposures and Lung Aging: Molecular Mechanisms and Implications for Improving Respiratory Health. Curr. Environ. Health Rep. *8*, 281–293.

32. Lopez-Otin, C., Blasco, M.A., Partridge, L., Serrano, M., and Kroemer, G. (2023). Hallmarks of aging: An expanding universe. Cell *186*, 243–278.

33. Ma, S., Ji, Z., Zhang, B., Geng, L., Cai, Y., Nie, C., Li, J., Zuo, Y., Sun, Y., Xu, G., et al. (2024). Spatial transcriptomic landscape unveils immunoglobin-associated senescence as a hallmark of aging. Cell *187*, 7025–7044.e34.

34. Goeminne, L.J.E., Vladimirova, A., Eames, A., Tyshkovskiy, A., Argentieri, M.A., Ying, K., Moqri, M., and Gladyshev, V.N. (2025). Plasma protein-based organ-specific aging and mortality models unveil diseases as accelerated aging of organismal systems. Cell Metab. *37*, 205–222.e6.

35. Argentieri, M.A., Xiao, S., Bennett, D., Winchester, L., Nevado-Holgado, A.J., Ghose, U., Albukhari, A., Yao, P., Mazidi, M., Lv, J., et al. (2024). Proteomic aging clock predicts mortality and risk of common age-related diseases in diverse populations. Nat. Med. *30*, 2450–2460.

36. Oh, H.S.H., Rutledge, J., Nachun, D., Pálovics, R., Abiose, O., Moran-Losada, P., Channappa, D., Urey, D.Y., Kim, K., Sung, Y.J., et al. (2023). Organ aging signatures in the plasma proteome track health and disease. Nature *624*, 164–172.

37. Davey Smith, G., and Hemani, G. (2014). Mendelian randomization: genetic anchors for causal inference in epidemiological studies. Hum. Mol. Genet. *23*, R89–R98.

38. Emdin, C.A., Khera, A.V., and Kathiresan, S. (2017). Mendelian Randomization. JAMA *318*, 1925–1926.

39. Eldjarn, G.H., Ferkingstad, E., Lund, S.H., Helgason, H., Magnusson, O.T., Gunnarsdottir, K., Olafsdottir, T.A., Halldorsson, B.V., Olason, P.I., Zink, F., et al. (2023). Large-scale plasma proteomics comparisons through genetics and disease associations. Nature *622*, 348–358.

40. Cao, Y., Wang, Y., Zhou, Z., Pan, C., Jiang, L., Zhou, Z., Meng, Y., Charugundla, S., Li, T., Allayee, H., et al. (2022). Liver-heart cross-talk mediated by coagulation factor XI protects against heart failure. Science *377*, 1399–1406.

41. Nelson, M.R., Tipney, H., Painter, J.L., Shen, J., Nicoletti, P., Shen, Y., Floratos, A., Sham, P.C., Li, M.J., Wang, J., et al. (2015). The support of

human genetic evidence for approved drug indications. Nat. Genet. *47*, 856–860.

42. Trajanoska, K., Bhérer, C., Taliun, D., Zhou, S., Richards, J.B., and Mooser, V. (2023). From target discovery to clinical drug development with human genetics. Nature *620*, 737–745.
43. Greer, P. (2002). Closing in on the biological functions of Fps/Fes and Fer. Nat. Rev. Mol. Cell Biol. *3*, 278–289.
44. Olvedy, M., Tisserand, J.C., Luciani, F., Boeckx, B., Wouters, J., Lopez, S., Rambow, F., Aibar, S., Thienpont, B., Barra, J., et al. (2017). Comparative oncogenomics identifies tyrosine kinase FES as a tumor suppressor in melanoma. J. Clin. Investig. *127*, 2310–2325.
45. Karamanavi, E., McVey, D.G., van der Laan, S.W., Stanczyk, P.J., Morris, G.E., Wang, Y., Yang, W., Chan, K., Poston, R.N., Luo, J., et al. (2022). The FES Gene at the 15q26 Coronary-Artery-Disease Locus Inhibits Atherosclerosis. Circ. Res. *131*, 1004–1017.
46. Tolomeo, P., Butt, J.H., Kondo, T., Campo, G., Desai, A.S., Jhund, P.S., Køber, L., Lefkowitz, M.P., Rouleau, J.L., Solomon, S.D., et al. (2023). Importance of cystatin C in estimating glomerular filtration rate: the PARADIGM-HF trial. Eur. Heart J. *44*, 2202–2212.
47. Glass, O., Henao, R., Patel, K., Guy, C.D., Gruss, H.J., Syn, W.K., Moylan, C.A., Streilein, R., Hall, R., Mae Diehl, A., and Abdelmalek, M.F. (2018). Serum Interleukin-8, Osteopontin, and Monocyte Chemoattractant Protein 1 Are Associated With Hepatic Fibrosis in Patients With Nonalcoholic Fatty Liver Disease. Hepatol. Commun. *2*, 1344–1355.
48. Remmerie, A., Martens, L., Thone, T., Castoldi, A., Seurinck, R., Pavie, B., Roels, J., Vanneste, B., De Prijck, S., Vanhockerhout, M., et al. (2020). Osteopontin Expression Identifies a Subset of Recruited Macrophages Distinct from Kupffer Cells in the Fatty Liver. Immunity *53*, 641–657.e614.
49. Ying, K., Liu, H., Tarkhov, A.E., Sadler, M.C., Lu, A.T., Moqri, M., Horvath, S., Kutalik, Z., Shen, X., and Gladyshev, V.N. (2024). Causality-enriched epigenetic age uncouples damage and adaptation. Nat. Aging *4*, 231–246.
50. Suhre, K. (2024). Genetic associations with ratios between protein levels detect new pQTLs and reveal protein-protein interactions. Cell Genom. *4*, 100506.
51. Chen, Y., Lu, T., Pettersson-Kymmer, U., Stewart, I.D., Butler-Laporte, G., Nakanishi, T., Cerani, A., Liang, K.Y.H., Yoshiji, S., Willett, J.D.S., et al. (2023). Genomic atlas of the plasma metabolome prioritizes metabolites implicated in human diseases. Nat. Genet. *55*, 44–53.
52. McCartney, D.L., Min, J.L., Richmond, R.C., Lu, A.T., Sobczyk, M.K., Davies, G., Broer, L., Guo, X., Jeong, A., Jung, J., et al. (2021). Genome-wide association studies identify 137 genetic loci for DNA methylation biomarkers of aging. Genome Biol. *22*, 194.
53. Deelen, J., Evans, D.S., Arking, D.E., Tesi, N., Nygaard, M., Liu, X., Wojczynski, M.K., Biggs, M.L., van der Spek, A., Atzmon, G., et al. (2019). A meta-analysis of genome-wide association studies identifies multiple longevity genes. Nat. Commun. *10*, 3669.
54. Kurki, M.I., Karjalainen, J., Palta, P., Sipilä, T.P., Kristiansson, K., Donner, K.M., Reeve, M.P., Laivuori, H., Aavikko, M., Kaunisto, M.A., et al. (2023). FinnGen provides genetic insights from a well-phenotyped isolated population. Nature *613*, 508–518.
55. Rao, M., Wang, X., Guo, G., Wang, L., Chen, S., Yin, P., Chen, K., Chen, L., Zhang, Z., Chen, X., et al. (2021). Resolving the intertwining of inflammation and fibrosis in human heart failure at single-cell level. Basic Res. Cardiol. *116*, 55.
56. Leblanc, F.J.A., Jin, X., Kang, K., Lee, C.J.M., Xu, J., Xuan, L., Ma, W., Belhaj, H., Benzaki, M., Mehta, N., et al. (2024). Atrial fibrillation variant-to-gene prioritization through cross-ancestry eQTL and single-nucleus multiomic analyses. iScience *27*, 110660.
57. Bulik-Sullivan, B., Finucane, H.K., Anttila, V., Gusev, A., Day, F.R., Loh, P. R., and ReproGen Consortium; Psychiatric Genomics Consortium; and Duncan, L.; Genetic Consortium for Anorexia Nervosa of the Wellcome Trust Case Control Consortium 3 (2015). An atlas of genetic correlations across human diseases and traits. Nat. Genet. *47*, 1236–1241.
58. Werme, J., van der Sluis, S., Posthuma, D., and de Leeuw, C.A. (2022). An integrated framework for local genetic correlation analysis. Nat. Genet. *54*, 274–282.
59. Giambartolomei, C., Vukcevic, D., Schadt, E.E., Franke, L., Hingorani, A. D., Wallace, C., and Plagnol, V. (2014). Bayesian test for colocalisation between pairs of genetic association studies using summary statistics. PLoS Genet. *10*, e1004383.
60. Purcell, S., Neale, B., Todd-Brown, K., Thomas, L., Ferreira, M.A.R., Bender, D., Maller, J., Sklar, P., de Bakker, P.I.W., Daly, M.J., and Sham, P.C. (2007). PLINK: a tool set for whole-genome association and population-based linkage analyses. Am. J. Hum. Genet. *81*, 559–575.
61. Grotzinger, A.D., Rhemtulla, M., de Vlaming, R., Ritchie, S.J., Mallard, T. T., Hill, W.D., Ip, H.F., Marioni, R.E., McIntosh, A.M., Deary, I.J., et al. (2019). Genomic structural equation modelling provides insights into the multivariate genetic architecture of complex traits. Nat. Hum. Behav. *3*, 513–525.
62. Watanabe, K., Taskesen, E., van Bochoven, A., and Posthuma, D. (2017). Functional mapping and annotation of genetic associations with FUMA. Nat. Commun. *8*, 1826.
63. Hemani, G., Tilling, K., and Davey Smith, G. (2017). Orienting the causal relationship between imprecisely measured traits using GWAS summary data. PLoS Genet. *13*, e1007081.
64. Hao, Y., Hao, S., Andersen-Nissen, E., Mauck, W.M., 3rd, Zheng, S., Butler, A., Lee, M.J., Wilk, A.J., Darby, C., Zager, M., et al. (2021). Integrated analysis of multimodal single-cell data. Cell *184*, 3573–3587.e29.
65. Wu, T., Hu, E., Xu, S., Chen, M., Guo, P., Dai, Z., Feng, T., Zhou, L., Tang, W., Zhan, L., et al. (2021). clusterProfiler 4.0: A universal enrichment tool for interpreting omics data. Innovation *2*, 100141.
66. Subramanian, A., Tamayo, P., Mootha, V.K., Mukherjee, S., Ebert, B.L., Gillette, M.A., Paulovich, A., Pomeroy, S.L., Golub, T.R., Lander, E.S., and Mesirov, J.P. (2005). Gene set enrichment analysis: a knowledge-based approach for interpreting genome-wide expression profiles. Proc. Natl. Acad. Sci. USA *102*, 15545–15550.
67. Szklarczyk, D., Kirsch, R., Koutrouli, M., Nastou, K., Mehryary, F., Hachilif, R., Gable, A.L., Fang, T., Doncheva, N.T., Pyysalo, S., et al. (2023). The STRING database in 2023: protein-protein association networks and functional enrichment analyses for any sequenced genome of interest. Nucleic Acids Res. *51*, D638–D646.
68. Shannon, P., Markiel, A., Ozier, O., Baliga, N.S., Wang, J.T., Ramage, D., Amin, N., Schwikowski, B., and Ideker, T. (2003). Cytoscape: a software environment for integrated models of biomolecular interaction networks. Genome Res. *13*, 2498–2504.
69. International HapMap 3 Consortium; Altshuler, D.M., Gibbs, R.A., Peltonen, L., Altshuler, D.M., Gibbs, R.A., Peltonen, L., Dermitzakis, E., Schaffner, S.F., Yu, F., et al. (2010). Integrating common and rare genetic variation in diverse human populations. Nature *467*, 52–58.
70. Mallard, T.T., Linnér, R.K., Grotzinger, A.D., Sanchez-Roige, S., Seidlitz, J., Okbay, A., de Vlaming, R., Meddens, S.F.W., Bipolar Disorder Working Group of the Psychiatric Genomics Consortium; and Palmer, A.A., et al. (2022). Multivariate GWAS of psychiatric disorders and their cardinal symptoms reveal two dimensions of cross-cutting genetic liabilities. Cell Genom. *2*, 100140.
71. Li, Z., Xiong, J., Guo, Y., Tang, H., Guo, B., Wang, B., Gao, D., Dong, Z., and Tu, Y. (2023). Effects of diabetes mellitus and glycemic traits on cardiovascular morpho-functional phenotypes. Cardiovasc. Diabetol. *22*, 336.
72. Burgess, S., Dudbridge, F., and Thompson, S.G. (2016). Combining information on multiple instrumental variables in Mendelian randomization: comparison of allele score and summarized data methods. Stat. Med. *35*, 1880–1906.

73. Bowden, J., Davey Smith, G., Haycock, P.C., and Burgess, S. (2016). Consistent Estimation in Mendelian Randomization with Some Invalid Instruments Using a Weighted Median Estimator. Genet. Epidemiol. *40*, 304–314.

74. Bowden, J., Davey Smith, G., and Burgess, S. (2015). Mendelian randomization with invalid instruments: effect estimation and bias detection through Egger regression. Int. J. Epidemiol. *44*, 512–525.

75. Burgess, S., and Thompson, S.G. (2015). Multivariable Mendelian randomization: the use of pleiotropic genetic variants to estimate causal effects. Am. J. Epidemiol. *181*, 251–260.

76. Ashburner, M., Ball, C.A., Blake, J.A., Botstein, D., Butler, H., Cherry, J.M., Davis, A.P., Dolinski, K., Dwight, S.S., Eppig, J.T., et al. (2000). Gene ontology: tool for the unification of biology. The Gene Ontology Consortium. Nat. Genet. *25*, 25–29.

77. Gene Ontology Consortium; Aleksander, S.A., Balhoff, J., Carbon, S., Cherry, J.M., Drabkin, H.J., Ebert, D., Feuermann, M., Gaudet, P., Harris, N.L., et al. (2023). The Gene Ontology knowledgebase in 2023. Genetics *224*, iyad031.

78. Kanehisa, M., and Goto, S. (2000). KEGG: kyoto encyclopedia of genes and genomes. Nucleic Acids Res. *28*, 27–30.

STAR★METHODS

KEY RESOURCES TABLE

REAGENT or RESOURCE	SOURCE	IDENTIFIER
Deposited data		
Proteomics data from the Iceland	Ferkingstad et al.[16]	https://www.decode.com/summarydata
Proteomics data from the Fenland	Pietzner et al.[17]	http://www.omicscience.org/apps/pgwas
Proteomics data from the UKB-PPP	Sun et al.[18]	https://metabolomips.org/ukbbpgwas/
Proteomics data from the UKB-PPP (ratios between protein levels)	Suhre[50]	https://www.ebi.ac.uk/gwas/home
Transcriptomics data from the eQTLGen Consortium	Võsa et al.[15]	https://www.eqtlgen.org
Transcriptomics data from the CAGE study	Lloyd-Jones et al.[13]	https://shiny.cnsgenomics.com/CAGE
Transcriptomics data from the GTEx Consortium	GTEx Consortium[14]	https://www.gtexportal.org/home
Epigenomics data from the LBC&BSGS cohort	McRae et al.[12]	https://datashare.ed.ac.uk/handle/10283/3645
Epigenomics data from the GTEx Consortium	Oliva et al.[22]	https://gtexportal.org/home/
Metabolomics data from the CLSA cohort	Chen et al.[51]	https://www.ebi.ac.uk/gwas/home
Epigenetic age acceleration	McCartney et al.[52]	https://datashare.ed.ac.uk/handle/10283/3645
Organ-specific biological age gap	Wen et al.[10]	https://labs-laboratory.com/medicine/
Frailty index	Atkins et al.[27]	https://figshare.com/articles/dataset/Genome-Wide_Association_Study_of_the_Frailty_Index_-_Atkins_et_al_2019/9204998
Healthy aging	Timmers et al.[24]	https://datashare.ed.ac.uk/handle/10283/3599
Healthspan	Zenin et al.[23]	https://zenodo.org/records/1302861
Lifespan	Timmers et al.[26]	https://datashare.ed.ac.uk/handle/10283/3209
Longevity	Deelen et al.[53]	https://www.longevitygenomics.org/downloads
Perceived age	Roberts et al.[25]	https://data.bris.ac.uk/data/dataset/21crwsnj4xwjm2g4qi8chathha
Overall health rating	Neale Lab	https://www.nealelab.is/uk-biobank
Aging-GIP1 and Aging-GIP1-adj	Timmers et al.[28]	https://datashare.ed.ac.uk/handle/10283/3817
Binary phenotypes from the UK Biobank	UK Biobank	https://pheweb.org/UKB-SAIGE
Binary phenotypes from the FinnGen Biobank	FinnGen[54]	https://www.finngen.fi/en/access_results
Normal and failing human hearts scRNA-seq dataset	Rao et al.[55]	GEO: GSE145154
Atrial fibrillation and sinus rhythm snRNA-seq dataset	Leblanc et al.[56]	GEO: GSE238242
Agora	The NIA-funded AMP-AD consortium	https://www.synapse.org/Synapse:syn13363443
Summary statistics for multivariate GWAS of $F_{cluster1}$, $F_{cluster2}$ and $F_{cluster3}$	This paper	https://aging-apps.shinyapps.io/heterogeneous-aging
Software and algorithms		
Python 3.8	Python Software Foundation	https://www.python.org
R 4.2.2	The R Foundation	https://www.r-project.org
LDSC 2.0.0	Bulik-Sullivan et al.[57]	https://github.com/bulik/ldsc
LAVA 0.1.0	Werme et al.[58]	https://github.com/josefin-werme/LAVA
SMR 1.3.1	Zhu et al.[21]	https://yanglab.westlake.edu.cn/software/smr
Coloc 5.2.3	Giambartolomei et al.[59]	https://github.com/chr1swallace/coloc
PLINK 1.9	Purcell et al.[60]	https://www.cog-genomics.org/plink
GenomicSEM 0.0.5	Grotzinger et al.[61]	https://github.com/GenomicSEM/GenomicSEM
FUMA 1.8.0	Watanabe et al.[62]	https://fuma.ctglab.nl/

(*Continued on next page*)

Continued

REAGENT or RESOURCE	SOURCE	IDENTIFIER
easyfinemap 0.4.4	Jianhua Wang	https://github.com/Jianhua-Wang/easyfinemap
TwoSampleMR 0.5.7	Hemani et al.[63]	https://github.com/MRCIEU/TwoSampleMR
Seurat 4.3.0	Hao et al.[64]	https://github.com/satijalab/seurat
clusterProfiler 4.10.1	Wu et al.[65]	https://github.com/YuLab-SMU/clusterProfiler
CMPlot 4.5.1	Yin et al.	https://github.com/YinLiLin/CMplot
GSEA	Subramanian et al.[66]	https://www.gsea-msigdb.org/gsea/index.jsp
STRING 12.0	Szklarczyk et al.[67]	https://string-db.org
Cytoscape 3.10.3	Shannon et al.[68]	https://cytoscape.org
Other		
Interactive visualization application of heterogeneous aging	This paper	https://aging-apps.shinyapps.io/heterogeneous-aging

EXPERIMENTAL MODEL AND SUBJECT DETAILS

The summary-level GWAS data used in this study were derived from populations of European ancestry.[10,12–18,22–28,50–54] All studies that provided data for these analyses were approved by the relevant institutional review boards in their respective countries, with informed consent from all participants. Detailed cohort characteristics of these data (including ethnic and geographic information) are provided in Table S1.

METHOD DETAILS

Global genetic correlation analysis

Global genetic correlation between blood-based epigenetic age acceleration and organ-specific biological age gap was estimated using LD score regression analysis.[57] European ancestry samples from the 1000 Genomes Project (Phase 3) were utilized as the reference panel.[69] To reduce statistical noise, SNPs with imputation quality scores below 0.9 or minor allele frequencies below 5% were excluded from the analysis.

Local genetic correlation analysis

Local genetic correlation between blood-based epigenetic age acceleration and organ-specific biological age gap was calculated using LAVA analysis.[58] First, data dividing the human genome into 2,495 semi-independent blocks was downloaded from the LAVA website (https://github.com/cadeleeuw/lava-partitioning). These semi-independent LD blocks are systematically partitioned genomic regions constructed based on LD information between SNPs. The partitioning methodology minimizes LD between blocks while maintaining approximately equal block sizes, thereby ensuring the relative independence of individual blocks. To quantify the local genetic correlation for each pair of phenotypes and remove unrelated loci, we first tested the local univariate joint association signal for each phenotype. For loci that had univariate associations with $p < 2 \times 10^{-5}$ (0.05/2495) for both phenotypes, further bivariate local genetic correlation testing was performed.

Druggable genome data

The druggable genome is derived from a recent study that integrates GWAS findings with data from the ChEMBL and First Databank databases.[20] This genome is categorized into three tiers corresponding to position in the drug-development pipeline. Tier 1 includes targets of approved small molecules and biotherapeutic drugs as well as clinical-phase drug candidates. Tier 2 encompasses genes encoding targets with known bioactive drug-like small molecule binding partners as well as those with $\geq$ 50% identity (over $\geq$ 75% of the sequence) with approved drug targets. Tier 3 comprises genes encoding secreted or extracellular proteins, proteins with more distant similarity to approved drug targets, and members of key druggable gene families not already included in Tiers 1 or 2.

SMR & HEIDI analysis

We employed the SMR & HEIDI methods to investigate the putative causal associations between the methylation, expression levels, and protein abundance of druggable genes and both blood-based epigenetic age acceleration and organ-specific biological age gap. The SMR & HEIDI methodologies leverage summary data from GWAS and QTL studies to assess whether the exposure and outcome phenotypes exhibit correlation attributable to shared causal variants.[21] In comparison to conventional MR, this method demonstrates enhanced capacity to differentiate between pleiotropic model (i.e., the exposure and the outcome are associated owing to a single shared genetic variant) and linkage model (i.e., there are two or more genetic variants in LD affecting the exposure

and outcome independently) through comprehensive analysis of top-associated cis-QTLs, thereby yielding higher statistical power. We selected the most statistically significant cis-QTL ($p < 5 \times 10^{-8}$) within a ±1000 kb window centered on each target gene for analysis. To ensure data quality, we excluded SNPs with allele frequency differences greater than 0.2 between any pair of datasets (encompassing LD reference samples, QTL summary statistics, and outcome summary data). We implemented the HEIDI test to distinguish between pleiotropic and linkage effects, with associations demonstrating $p\_HEIDI < 0.05$ being considered potentially pleiotropic and subsequently excluded from further analysis. To control the false discovery rate (FDR), we adjusted the p values using the Benjamini-Hochberg method, controlling the FDR at 0.05. Associations meeting the criteria of $FDR\_SMR < 0.05$ and $p\_HEIDI > 0.05$ were deemed statistically significant and subjected to subsequent in-depth analysis.

Colocalization analysis

We performed colocalization analyses to determine if the identified associations of proteins, genes, and DNAm sites with blood-based epigenetic age acceleration and organ-specific biological age gap shared the same causal variant. These analyses were conducted using a Bayesian-based method implemented in the R package coloc.[59] The colocalization analysis reports posterior probabilities for five mutually exclusive hypotheses: (1) no causal variants for either of the two traits (H0); (2) a causal variant for trait 1 only (H1); (3) a causal variant for trait 2 only (H2); (4) distinct causal variants for two traits (H3); and (5) the same shared causal variant for both traits (H4). We considered pairs of molecular traits with a posterior probability for hypothesis 4 (PP-H4) greater than 0.8 as showing significant colocalization.

Clustering analysis

Hierarchical clustering was performed to classify heterogeneous aging-related phenotypes based on their associations with DNAm, gene expression, and protein abundance. Specifically, Ward's linkage was employed to construct a dendrogram based on the correlation patterns between phenotypes and molecular signatures. The optimal number of clusters was determined through examination of the dendrogram topology. Subsequently, principal component analysis was applied for dimensionality reduction and visualization of the high-dimensional data to reveal the distributional characteristics of distinct phenotypic clusters among these heterogeneous aging-related phenotypes.

Gene set enrichment analysis

To further elucidate the biological characteristics of heterogeneous aging-related phenotypic clusters, we performed gene set enrichment analysis[66] to systematically evaluate pathway alterations across the three phenotypic clusters. Using the clusterProfiler R package,[65] we conducted Gene Ontology enrichment analysis to identify significantly enriched biological processes and their normalized enrichment scores within each aging-related phenotype. To determine cluster-specific pathways, we compared enrichment scores between each target cluster and the remaining clusters using the Wilcoxon ranked-sum test. P values were adjusted using the Benjamini-Hochberg method.

Genomic SEM

We employed genomic SEM implemented in the Genomic SEM R package to conduct multivariate GWAS on cluster-related aging phenotypes, investigating the shared genetic liability underlying these phenotypic clusters. A key advantage of this approach is that it is not biased by sample overlap (UK Biobank participants included in multiple input GWASs) or by imbalanced sample sizes.[61] Furthermore, genomic SEM also facilitates identification of variants only influencing some but not all of the complex traits, and which therefore do not represent a broad cross-trait liability.[61] The genomic SEM was performed in two stages.[61] At stage 1, we estimated the empirical genetic covariance matrix and its corresponding sampling covariance matrix using a multivariate extension of cross-trait LD score regression, based on GWAS for each cluster-related aging phenotype. At stage 2, we constructed a common factor model by estimating model parameters through minimizing the hypothesized covariance matrix and the empirical covariance matrix calculated in the first step. In the multivariate GWAS, we used the recommended default quality control parameters, which included removing SNPs with MAF < 0.01 (prone to error due to fewer samples within the genotype cluster and LD score regression standard errors for these SNPs tend to be high), SNPs with effect estimates exactly equal to zero (so as to avoid compromising matrix inversion necessary for genomic SEM), SNPs not matching the 1000 Genomes Phase 3 EUR reference panel and SNPs with mismatched alleles.[61] Following quality control, applying the common factor SEM specification, the individual autosomal SNP associations are incorporated into the genetic and associated sample covariance matrices to generate the multivariate GWAS result reflecting shared genetic variation across the input GWASs. The effective sample size of common factor was estimated according to the method proposed by Mallard et al., utilizing SNPs with MAF ranging from 10% to 40% to obtain more robust estimates.[70]

Q_{SNP} heterogeneity

To evaluate the potential heterogeneity of SNP effects across different cluster-related aging phenotypes, we employed genome-wide Q_{SNP} statistics for heterogeneity testing.[61] The null hypothesis of this test assumes that the effect of an SNP operates through a latent factor (that is, the common pathway model). Deviations from this null hypothesis indicate that the model with direct SNP effects on the indicators (that is, the independent pathway model) provides a better explanation. Q_{SNP} statistics were derived from the χ^2 difference test comparing the common and independent pathway models.

Identification of genomic loci and variants

FUMA was used to identify genomic loci and lead SNPs in LD ($R^2 < 0.1$) associated with the common factor at genome-wide significance ($p < 5 \times 10^{-8}$), perform functional annotation, and conduct functional gene mapping.[62] We defined a locus by lead SNPs within a 500 kb range and all SNPs in high LD ($R^2 > 0.6$) with at least one independent SNP. We also compared lead SNPs with the original univariate GWAS and defined SNPs to be novel if they were > 1 Mb from SNPs identified in the univariate GWAS data.

Fine mapping

We employed five fine mapping methods (ABF, PAINTOR, CAVIARBF, FINEMAP, and SuSiE) through the Python pipeline easyfinemap (https://jianhua-wang.github.io/easyfinemap/) to identify the most plausible causal variants within genomic loci associated with the common factor. Specifically, we analyzed regions of interest by incorporating all variants within a 500 kb window upstream and downstream of the lead SNPs from the common factor GWAS. Fine mapping analysis was performed on these regions of interest, with the maximum output constrained to one SNP per region to enable identification of variants with the highest causal probability.

Identification of cross-layer molecular regulatory networks

The systematic integration of epigenomic, transcriptomic, and proteomic data facilitates the elucidation of gene regulatory networks across multiple molecular levels. For significant candidate causal molecules with colocalization evidence associated with heterogeneous aging-related phenotypes, we employed SMR & HEIDI analysis to examine potential causal associations between DNAm and gene expression, DNAm and protein abundance, as well as gene expression and protein abundance. We retained causal associations that passed statistical significance thresholds (FDR_SMR < 0.05 and p_HEIDI > 0.05).

Tissue-specific analysis

Alterations in plasma protein abundance may originate from diverse tissues. To elucidate the underlying mechanisms of the observed associations between the plasma proteome and blood-based epigenetic age acceleration, as well as organ-specific biological age gap, we conducted a comprehensive re-analysis utilizing SMR & HEIDI methods.[21] This analytical approach incorporated tissue-specific datasets derived from 48 non-peripheral blood tissues catalogued in the GTEx database.[14] This step aimed to verify the consistency of these effects across different tissues and further evaluate potential off-target effects of drugs targeting specific genes.

Multivariate longevity phenotype analysis

To investigate whether plasma proteins that are significantly associated with blood-based epigenetic age acceleration and organ-specific biological age gap have potential causal effects on more clinically relevant complex aging traits, we employed the SMR & HEIDI methods to test the associations between these proteins and nine phenotypes characterizing distinct aspects of aging and longevity.[23–28,53] Subsequently, based on their observed effects, we stratified these proteins into three categories: those exhibiting heterogeneous effects, those demonstrating pro-longevity effects, and those manifesting anti-longevity effects.

Phenome-wide association study

To evaluate the pleiotropic effects and potential adverse outcomes associated with putative therapeutic targets, we conducted a PheWAS utilizing an extensive array of binary phenotypes derived from the UKB-SAIGE repository. The original database included 1,403 traits, categorized according to the ICD codes, all of which were analyzed employing the SAIGE method. To ensure robust statistical power, we selectively included 1,075 traits with more than 200 cases and performed PheWAS on these phenotypes. For independent validation, FinnGen Biobank phenotypes were matched with UK Biobank phenotypes based on ICD codes, and phenotypes with more than 200 cases were selected for subsequent PheWAS.

Metabolome-wide Mendelian randomization

To elucidate the metabolomic determinants influencing blood-based epigenetic age acceleration and organ-specific biological age gap, we performed a two-sample MR analysis on 283 plasma metabolic traits.[51] Initially, we identified SNPs associated with metabolites using a genome-wide significance threshold ($p < 5 \times 10^{-8}$). Subsequently, SNPs underwent clumping for LD using PLINK, implementing a strict cutoff of clumping threshold of $R^2 < 0.001$ within a 10,000 kb window.[60] To check for weak instrument bias among the remaining SNPs, we calculated F-statistics using established methodologies from previous studies, excluding SNPs with F-values below 10.[71] In the MR analysis, we initially harmonized the exposure and outcome data and employed the Steiger filtering method to eliminate inappropriate SNPs, thereby mitigating reverse causation. The harmonized data ensures that each metabolite has more than three independent instrumental variables, meeting the statistical power requirements and enabling subsequent sensitivity analyses. IVW served as the primary statistical method.[72] Additionally, multiple methodologies were implemented, including MR-Egger and weighted median method.[73,74] To assess heterogeneity, we employed Cochran's Q test. When heterogeneity was evident, a random-effects IVW method was utilized, otherwise a fixed-effects IVW method was adopted. We evaluated the potential for reverse causality between exposure-outcome pairs using the MR Steiger directionality test.[63] Lastly, we conducted the Egger intercept test to detect horizontal pleiotropy.[74] To mitigate the risk of false positives due to multiple hypothesis testing, we applied the Benjamini-Hochberg method to calculate FDR-adjusted p values, considering results with an FDR < 0.05 as statistically significant. Given that high genetic correlations among metabolites might lead to multicollinearity, metabolites identified as significant

through univariate MR underwent further MVMR analysis. MVMR offers advantages in effectively managing the complexities arising from interdependencies between genetic variants associated with diverse exposures by including multiple exposures that interact.[75] For each heterogeneous aging-related phenotype, MVMR was performed employing all instrumental variables associated with significant metabolites identified in univariate MR analysis. The results of the MVMR-IVW analysis represent our primary findings, with statistical significance determined at an adjusted FDR < 0.05. For metabolites identified as significant through MVMR, we further investigated the regulatory relationships between these plasma metabolites and the DNAm sites, genes, and circulating proteins that mediate heterogeneous aging. Statistically significant associations with adjusted FDR < 0.05 were visualized using Cytoscape software.[68]

Downstream effects mediated by heterogeneous aging

To elucidate downstream biological effects mediated by blood-based epigenetic aging and organ-specific aging, we performed two-sample MR analyses. These analyses leveraged proteomic data from the Iceland, Fenland, and UKB-PPP cohorts, as well as metabolomic data from the CLSA cohort.[16–18,51] In the analytical framework, we posited blood-based epigenetic aging and organ-specific aging as exposures, with proteomic and metabolomic signatures serving as outcomes. Unless explicitly stated otherwise, the protocols for harmonization, clumping, instrument selection, and MR methods and estimators were the same as those used for our metabolome-wide MR. Given that the number of genetic instrumental variables for all exposures exceeded the minimum threshold of two, we employed the IVW, MR-Egger, and weighted median method for analysis and performed corresponding sensitivity analyses.

Single-cell RNA sequencing and single-nucleus RNA sequencing analyses

Single-cell RNA sequencing and single-nucleus RNA sequencing were conducted using publicly available datasets. The study analyzed left ventricular tissues from patients with ischemic cardiomyopathy and healthy donors, as well as left atrial appendage tissues from patients with atrial fibrillation and corresponding healthy controls. Detailed protocols for tissue sample acquisition are described in the respective original research publications.[55,56] The sequencing process was performed using the 10x Genomics platform for both single-cell RNA sequencing and single-nucleus RNA sequencing. The data analysis workflow, including downstream processing, quality control, and cell type annotation, was implemented in accordance with the methodologies reported in the original publications of each project.[55,56] To explore potential cell-specific targets associated with disease states, we performed differential gene expression analysis using the FindMarkers function in Seurat package.[64]

Functional enrichment analysis

Using the clusterProfiler R package.[65] we performed functional enrichment analysis on the identified druggable protein-coding genes to elucidate their biological functions and associated pathways. We conducted the analysis based on Gene Ontology and Kyoto Encyclopedia of Genes and Genomes pathway databases.[76–78] We applied the Benjamini-Hochberg method to correct the false discovery rate in multiple testing, considering an FDR < 0.05 as statistically significant.

Protein-protein interaction network analysis

To characterize the interactions among the identified proteins, we conducted protein-protein interaction network analysis. We utilized curated protein-protein interaction data and predicted functional associations from the STRING database to determine known and potential relationships between proteins.[67] The analysis was performed using default parameter settings, with the minimum interaction score threshold set to 0.4.

QUANTIFICATION AND STATISTICAL ANALYSIS

The quantitative and statistical analyses are described thoroughly in the relevant sections of the method details. Unless otherwise specified, to minimize the risk of false positives due to multiple hypothesis testing, we calculated FDR-adjusted *p* values using the Benjamini-Hochberg method, with results considered statistically significant at FDR < 0.05.